IEEE Access
Multidisciplinary | Rapid Review | Open Access Journal

Received 16 August 2024, accepted 30 August 2024, date of publication 2 September 2024, date of current version 12 September 2024.

Digital Object Identifier 10.1109/ACCESS.2024.3453755

RESEARCH ARTICLE

Terminal Voltage and Load Frequency Control in a Real Four-Area Multi-Source Interconnected Power System With Nonlinearities via OOBO Algorithm

TAYYAB ALI[1], MUHAMMAD ASAD[1], EZZEDDINE TOUTI[2], BESMA BECHIR GRABA[3], MOULOUD AOUDIA[4], GHULAM ABBAS[5], HAMMAD ALNUMAN[6], AND WALEED NURELDEEN[7]

[1]Department of Electrical and Computer Engineering, International Islamic University Islamabad, Islamabad 44000, Pakistan
[2]Department of Electrical Engineering, College of Engineering, Northern Border University, Arar 91431, Saudi Arabia
[3]Department of Physics, College of Science, Northern Border University, Arar 91431, Saudi Arabia
[4]Department of Industrial Engineering, College of Engineering, Northern Border University, Arar 91431, Saudi Arabia
[5]School of Electrical Engineering, Southeast University, Nanjing 210096, China
[6]Department of Electrical Engineering, College of Engineering, Jouf University, Sakaka 72388, Saudi Arabia
[7]College of Engineering, University of Business and Technology, Jeddah 21432, Saudi Arabia

Corresponding author: Ezzeddine Touti (esseddine.touti@nbu.edu.sa)

This work was supported by the Deanship of Scientific Research at Northern Border University, Arar, Saudi Arabia, under Project NBU-FFR-2024-2448-01.

ABSTRACT The increasing expansion of the industrial and domestic sectors, combined with the integration of renewable energy sources, has led to an overload of the existing interconnected power systems, which in turn has led to significant bottlenecks. This confluence of factors manifests itself in severe frequency, voltage and tie-line power issues, highlighting the urgent need for intelligent control mechanisms. Automatic voltage regulation (AVR) and load frequency control (LFC) are key components that ensure the supply of high-quality energy to consumers while maintaining the nominal frequency, voltage and power deviations in the grid. These measures are essential to ensure the stability and safety of the IPS under these challenging conditions. This research addresses the control strategies for a four-area sophisticated IPS. The complexity of the system, which includes five generation units in each area, including gas, thermal reheating, hydropower and two renewable energy sources (wind and photovoltaic), requires a careful study of the control methods. In particular, the inclusion of various non-linear factors, such as the governor dead band (GDB), generation rate constraint (GRC) and boiler dynamics (BD) in each of the four areas, increases the realism of the study. In this context, a recently introduced meta-heuristic algorithm, the One-to-One-based Optimizer (OOBO), was used to determine the optimal parameters of the proportional-integral-proportional-derivative (PI-PD) controller. The tuning process involves using the integral of time multiplied by the squared error value (ITSE) as the error criterion for evaluating the fitness function. In the study, the voltage, frequency and power performance of the OOBO PI-PD controller is evaluated and compared with alternative control methods, namely Proportional-Integral-Derivative (PID), Integral-Proportional (I-P) and Integral-Proportional-Derivative (I-PD) controllers, all of which are tuned with OOBO. Under the influence of a 5% load step load perturbation (SLP), comprehensive comparisons show the superior performance of the OOBO PI-PD controller, which shows better responses in all areas. Furthermore, the reliability and effectiveness of the OOBO PI-PD method are validated by a sensitivity analysis that considers simultaneous variations of the turbine time constant and speed control within a range of ±25%. The results highlight the robustness of the OOBO-PI-PD control

The associate editor coordinating the review of this manuscript and approving it for publication was Rossano Musca.

strategy and demonstrate its ability to effectively stabilize variations in terminal voltage, load frequency and tie-line power with a significantly shorter settling time within the complicated dynamics of a four-area IPS with nonlinearities.

INDEX TERMS Automatic voltage regulation, load frequency control, meta-heuristic optimization, one-to-one-based optimizer, PID controller, power system.

I. INTRODUCTION

A. BACKGROUND

Modern power grids are changing rapidly as more and more renewable energy sources and smart grid technologies are deployed. The most important control objective in interconnected power systems (IPSs) is to control the output power while ensuring that the deviations in frequency, terminal voltage, and tie line power are zero. In an IPS, automatic voltage regulators (AVR) and load frequency control (LFC) are essential for maintaining the rated voltage and frequency while ensuring a consistent and reliable power supply to the loads. Load dynamics in power systems are always dynamic, meaning that they are constantly changing. Unwanted fluctuations in grid frequency and voltage result from the mismatch between generation and load demand. Frequency deviation is controlled using an LFC loop by modifying the active power demand through speed governor action. By modifying reactive power demand through generator excitation, the AVR loop controls the terminal voltage deviation. The exchange of electrical power between different control areas is transmitted via tie-line connections. It is a difficult challenge to develop an intelligent and reliable control method that minimizes the fluctuations in tie-line power flow, system frequency, and terminal voltage [1], [2].

B. LITERATURE REVIEW

In the recent past, a lot of work has been presented regarding the effective control of LFC and AVR control loops. Ali et al., suggested LPBO-, AOA-, MPSO- and DO-based PI-PD controllers for different multi-area multi-source IPSs with and without nonlinearities for effective control of both terminal voltage and load frequency simultaneously [1], [2]. Using simulated annealing (SA) and conventional Ziegler-Nichols (ZN) approaches, Chandrakala and Balamurugun adjusted a PID controller to stabilize a two-area IPS, successfully regulating both load frequency and terminal voltage [3]. To improve time response for voltage and frequency stabilization in a single-area power system, Gupta and Srivastava looked into the hybrid NN-FTF controller [4]. For a single-area, single-source IPS, Devashish Sharma et al. suggested that ZN-based FLC and PID controllers achieve better dynamic response [5]. For a two-area, four-source nonlinear IPS, Rumi and Lalit investigated PIDF/PIDuF controllers based on LSA, and their findings demonstrated the superiority of fractional-order controllers with filters over conventional control techniques [6]. Deepak and Ajit studied MFO-based FOPID controllers to stabilize a two-area nonlinear IPS [7]. For a two-area, four-source IPS, A. K. Sahani et al. suggested a PID controller based on FA that was successful in stabilizing the power system [8]. Javed and Zahra proposed an IPSO-based CPSS controller that integrates hydro, thermal reheat, and gas production units for a single-area nonlinear IPS [9]. When IPFC, RFBs, and an HVDC link were added, Naga Sai Kalyan and Sambasivan's DE-AEFA-based PID control strategy for a two-area IPS with nonlinearities like GRC significantly improved [10], [11]. For AVR and LFC loops, respectively, Abhineet and Parida suggested SCA-based PI and PIDF controllers, with the added use of UPFC and RFB for further system response enhancements [12]. A PID controller for a two-area linear IPS optimized using NLTA was created by Nahas et al. [13]. To increase performance, Naga Sai Kalyan introduced a GWO-based PIDD controller for a two-area nonlinear IPS that included SMES and UPFC [14]. For a two-area, four-source IPS with nonlinearities, Anusha et al. examined a PID controller adjusted with FA and showed enhanced dynamic response [15].

To improve system performance, Oladipo et al. used a PIDA controller adjusted with hFPAPFA for a single-area, single-source IPS [16]. An HHO-tuned TIDF controller was proposed by researchers [17] for a two-source, three-area nonlinear IPS. The second-order error-driven control-law-based ADRC controller for a three-area IPS with EVs, solar, geothermal, and wind sources was investigated by Ali et al. [18]. For a three-area, two-source nonlinear IPS with dish-stirling, wind, solar, and reheat thermal production units, Satish Kumar Ramoji et al. recommended an HHO-based 2DOF I-TDF controller, outperforming other controllers in the process [19]. A CFPD-TID controller with GDB and GRC nonlinearities for a two-area, four-source nonlinear IPS with AFA was proposed by Ramoji [20].

Biswanath Dekaraja presented a CFOTDN-FOPDN controller for a two-area, four-source nonlinear IPS [21]. AFA-based CPDN-FOPIDN controller with GDB and GRC nonlinearities was used in a three-area IPS with GRC nonlinearities [22]. A PIDA controller employing DPO for a two-area, ten-source IPS with solar and bioenergy sources was examined by Hady H. Fayek and Eugen Rusu [23]. Using energy storage devices like RFBs, SMES, and UCs, Naga Sai Kalyan et al. investigated a HAEFA-based fuzzy PID for a two-area, three-source IPS. They successfully integrated the system into the LFC-AVR, with RFBs being better at attenuating frequency and voltage oscillations [24]. In [25], the gradient-based optimization (GBO) is used to fine-tune the parameters of the fuzzy proportional-integral-derivative-double derivative (FPIDD2) controller in a two-area IPS

TABLE 1. Nomenclature.

Acronym	Definition	Acronym	Definition
T_{rh}	Transient droop time constant	PI-PD	Proportional Integral Proportional Derivative
SLP	Step load perturbation	K_1, K_2, K_3, K_4,	Cross-coupling coefficients for AVR and LFC loops
PID	Proportional integral derivative	T_{CR}	Combustion reaction time delay
V_t	Terminal voltage	Y	Speed governor lag time constant
I-PD	Integral–proportional derivative	Δf	Frequency deviation
R_t, R_h, R_g, R_w	Speed regulation of thermal reheat, hydro, gas, and wind power plants	T_{12}, T_{13}, T_{14}, T_{21}, T_{23}, T_{24}, T_{31}, T_{32}, T_{34}, T_{41}, T_{42}, T_{43}	Tie-line synchronizing time constants
OOBO	One-to-one Based Optimized	K_p	Gain of power system
I-P	Integral–proportional	T_{CD}	Compressor discharge volume time constant
T_p	The time constant of the power system	X	Speed governor lead time constant
LFC	Load frequency control	T_w	Water time constant
ΔP_{tie}	Tie-line power deviation	K_{w1}, K_{w2}	Wind plant gain constants
AVR	Automatic voltage regulator	T_{w1}, T_{w2}	Wind turbine time constants
ΔP_D	Load deviation	T_{PV}	Solar PV time constant
IPS	Interconnected power system	K_{PV}	Solar PV gain constant
T_{tr}	The time constant of thermal turbine	a,b,c	Valve positional time constant
B	Area biasing factor	T_h	Main servo time constant
T_{re}	The time constant of reheat steam turbine	K_a	Gain of amplifier
T_a	The time constant of the amplifier	K_e	Gain of exciter
K_g	Gain of the generator field	T_e	The time constant of exciter
T_{gr}	The time constant of the speed governor	T_s	The time constant of the voltage sensor
K_{re}	Gain of reheat steam turbine	T_g	The time constant of the generator field
K_s	Gain of voltage sensor	T_f	Fuel time constant
D	Frequency-sensitive load coefficient	V_S	Sensor voltage
P_S	Synchronizing power coefficient	V_e	Error voltage
H	Inertia constant	GDB	Governor dead band
T_{rs}	Speed governor rest time	FTF	Fast traversal filter
GRC	Generation rate constraints	MFO	Moth Flame Optimization
SMES	Superconducting magnetic energy storage	DE	Differential Evolution
NN	Neural network	GWO	Grey Wolf Optimizer
FO	Fractional order	PFA	Pathfinder Algorithm
AOA	Archimedes Optimization Algorithm	NLTA	Nonlinear Threshold Accepting Algorithm
FA	Firefly Algorithm	CFPD	Cascaded Fuzzy PD
IPSO	Improved Particle Swarm Optimization	MPSO	Modified Particle Swarm Optimization
AEFA	Artificial Electric Field Algorithm	AFA	Artificial Flora Algorithm
ADRC	Active disturbance rejection control	UCs	Ultracapacitors
UPFC	Unified Power Flow Controller	CPSS	Conventional power system stabilizer
SCA	Sine Cosine Algorithm	LPBO	Learner Performance-Based Behavior Optimization
FPA	Flower Pollinated Algorithm	IPFC	Interline Power Flow Controller
HHO	Harris Hawks Optimization	DO	Dandelion Optimizer
CTD	Communication Time Delay	2DOF	Two degrees of freedom
DPO	Doctor and Patient Optimization Technique	ITSE	The integral of time multiplied by the squared value of the error
FPIDD^2	Fuzzy Proportional-Integral-Derivative-Double Derivative	FTIλDN	Fuzzy-Tilt-Fractional Order Integral-Filtered Derivative
MF	Membership Functions	ICA	Imperialist Competitive Algorithm

with various nonlinearities such as GRC, GDB, and communication time delay (CTD) to stabilize the voltage and frequency control loops. When the suggested FPIDD2 controller's response was compared to various control strategies, it was discovered that GBO-FPIDD2 had a comparatively better response in terms of load frequency deviation and terminal voltage. In [26], authors have recommended fuzzy-tilt-fractional order integral-filtered derivative (FTIλ DN) controller to optimize the load frequency and tie-lie power deviation in two- and five-area IPS with nonlinearities such as GRC and GDB. The suggested controller was tuned using an imperialist competitive algorithm (ICA). Moreover, asymmetrically spaced membership functions (MFs) have been employed to enhance the performance of the

FTIλDN controller. It can be noticed that the proposed control scheme provided satisfactory results in terms of better settling time, undershoot, and overshoot responses. To confirm the practicality of the proposed control scheme, a real-time hardware-in-the-loop simulation test has been successfully conducted. There is a large amount of research on individual LFC whereas there are relatively few studies on combined LFC-AVR. Several nature-inspired computation algorithms have been studied for the best control of the LFC loop of different IPSs [27], [28], [29], [30], [31], [32]. Moreover, a range of control strategies have been proposed for the individual control of the AVR loop [33], [34], [35], [36], [37]. Table 1 presents the summary of nomenclature used in this study whereas the summary of literature on AVR and LFC studies is provided in Table 2. In [38], authors have investigated a four-area multi-source IPS without nonlinearities using a based PID control scheme. They suggested that the proposed GBO-PID performed relatively better compared to other control methods. The results show that even with a 5% step load perturbation, the suggested GBO-PID controller works better than the alternatives, offering better responses in voltage, frequency, and tie-line power. Sensitivity analysis validates GBO-PID's dependability and effectiveness.

In [39], authors presented an intelligent energy management strategy for islanded networked microgrids (NMGs) in smart cities, addressing renewable energy uncertainties and power fluctuations. The approach combines an intelligent probabilistic wavelet fuzzy neural network with deep reinforcement learning (IPWFNN-DRLA) for active power and frequency control. The strategy employs a deep reinforcement learning framework, solved using the soft actor-critic algorithm, and operates in both offline training and decentralized distributed modes. The proposed model achieves over 98% accuracy, reduces computational burden by 7.82%, and cuts computation time by 61.1% compared to other methods [39]. The voltage and frequency stability in microgrids (MG) has been addressed in smart cities, focusing on uncertainties in operating conditions. An energy management platform using an intelligent probabilistic wavelet petri neuro-fuzzy inference algorithm (IPWPNFIA) is proposed to control V/F with renewable energy sources (RESs) and battery energy storage systems (BESS). The approach utilizes central and local controllers, asymmetric membership functions, and time-of-use demand response programs. The platform, verified via MATLAB/Simulink and RT-LAB, demonstrates fast dynamic response, real-time control, reduced calculation time, and effective coordination for protection equipment adjustment [40].

In [41], authors have introduced an energy management and control strategy for islanded DC microgrids with renewable energy sources (RES) and battery storage units (BU), considering the state of charge (SOC) of each BU. The model employs a sequential distributed energy management and multiple dynamic matrix model predictive control algorithm (MDMMPC) for power control by local controllers, prioritizing generation, and minimal communication. Simulation results cover various scenarios, and a hardware-in-the-loop (HIL) environment using a Micro Lab box and dSPACE control desk is demonstrated. The experimental setup ensures reduced converter fluctuations, and minimal overshoot, and features simplicity, rapidity, ease of operation, and distributed control [41]. A hierarchical, data-driven energy management approach has been presented for multi-integrated energy systems (MIES), incorporating renewable energy resources (RER), energy storage systems (ESSs), and integrated demand response (IDR) programs. The method aims to minimize operating costs, risk cost and environmental pollution using a multi-agent deep reinforcement learning (MADRL) model based on Markov decision processes and solved with multi-agent soft actor-critic and deep Q-learning algorithms. Results show reductions of 19.51% in operational costs, 19.69% in risk costs and 20.24% in pollution costs, demonstrating a fast, accurate, and computationally efficient solution for smart city energy management [42]. The optimal sizing and placement of energy storage systems (ESSs) have been demonstrated in microgrids (MGs) due to the rise of intermittent energy sources. It presents a multi-objective bi-level optimization problem, first determining the optimal size and capacity of battery energy storage systems (BESS) to minimize frequency fluctuations using stochastic daily data. The second level incorporates the dynamic behavior of MG elements, developing a dynamic objective function based on system eigenvalues and voltage sensitivity indices. The optimization, performed using an adaptive fuzzy particle swarm optimization (APT-FPSO) algorithm, aims to reduce power losses, enhance voltage stability, and mitigate low-frequency fluctuations. The approach's effectiveness is validated through time-domain simulations, voltage sensitivity studies, and eigenvalue analysis [43].

In [44], authors have addressed the challenge of frequency fluctuations in microgrids (MGs) with high renewable energy penetration by proposing an effective load frequency control (LFC) strategy. It integrates a wind turbine generator (WTG) with a diesel generator (DEG) in a diesel-wind energy-based microgrid (DWMG) and employs a PID frequency controller alongside an integral sliding mode control (I-SMC) for enhanced stability. An artificial gorilla troops optimizer (GTO) is used to fine-tune the controller parameters. The proposed approach demonstrates improved performance, including reduced frequency deviations, shorter settling times, and minimal integral errors compared to existing methods [44]. In [45], authors tackled the challenge of load frequency control (LFC) in a standalone micro-grid (S-μG) with high renewable penetration using a wild horse optimizer (WHO)-assisted intelligent fuzzy tilt integral derivative with filter – one plus integral (FTIDF-(1+I)) controller. The S-μG integrates solar photovoltaic, wind turbine, and diesel generators with a flywheel for energy storage. The proposed controller effectively manages the uncertainties and nonlinearities of the system, outperforming traditional methods

and other optimization algorithms like PSO and GWO. The results show significant reductions in frequency deviation, and the controller's robustness and stability are validated using the IEEE 39 bus system [45]. A novel load frequency control (LFC) scheme for a standalone microgrid (MG) using a marine predator algorithm (MPA)-assisted one plus proportional derivative with filter-fractional order proportional-integral ((1+PDF)-FOPI) controller has also been explored. The MG integrates photovoltaic, wind turbine, and diesel generators, along with ultracapacitors and flywheels for energy storage, addressing system mismatches due to stochastic loads and high renewable shares. The proposed controller outperforms traditional methods and optimization techniques, achieving a maximum frequency deviation of −0.016 Hz, well within IEEE standards. Real power system validation is performed using the modified New England IEEE-39 test bus system [46].

C. RESEARCH GAP AND MOTIVATION

Due to the highly complex structure of IPS, no research has been carried out on the combined control of LFC and AVR control loops in a four-area multi-sources IPS with nonlinearities such as GDB, GRC, and BD. This study fills this gap by examining a four-area IPS with five generation units per area, including three conventional and two renewable energy sources, including solar and wind power plants. The one-to-one-based optimizer (OOBO) is a recently discovered metaheuristic algorithm that has been successfully explored to improve the performance metrics of optimization problems. That is why, it is worth utilizing OOBO to obtain the optimum gain parameters of proposed PI-PD and other controllers including I-PD, I-P, and PID to achieve an effective response of four-area multi-source IPS.

D. CHALLENGES

The integration of renewable energy sources, such as wind and solar photovoltaic units presents different challenges due to their inherent variability and intermittency. Furthermore, the system becomes more complex due to the addition of several nonlinearities like BD, GRC, and GDB. These challenges include fluctuations in power generation levels, unpredictable output, and the need for effective control strategies to maintain the system's stability and reliability. The OOBO-based control strategies played a crucial role in addressing these challenges by enhancing the system's ability through intelligent parameter tuning and adaptive control mechanisms.

The following is a summary of this work's major contributions:

1. The modeling of four-area multi-sources IPS with nonlinearities and load perturbation.
2. The suggested PI-PD controller's mathematical modeling with four-area IPS.
3. The fitness functions formulation based on OOBO to find the optimal parameters of PI-PD and other controllers.
4. A comparative analysis of OOBO-PI-PD with other controllers such as OOBO-I-PD, OOBO-PID, and OOBO-I-P to justify the superiority of OOBO-PI-PD controller.
5. Sensitivity analysis has been carried out to validate the robustness of the proposed OOBO-PI-PD control strategy. For the proposed four-area IPS, adjustments in parameters are made within a range of about ±25%.

The structure of the research paper is as follows: The power system's structure is described in detail in Section II. Section III presents the details of the proposed control strategies. Section IV explains the workings of the suggested OOBO algorithm. Section V presents the outcomes of the experimental work and explanations of the results. Section 6 concludes the research, and it also tells the future research directions.

II. POWER SYSTEM MODELING

Figure 1(a) shows the generalized multi-source IPS model with integrated LFC and AVR control loops comprising nonlinearities. Cross-coupling between two loops is achieved with various coupling coefficients. Each of the four areas that make up the IPS has five sources: gas, hydro, solar photovoltaic, wind, and reheat thermal units. As seen in Figure 1(b), tie lines are used to connect different areas. Finally, the overall four-area interconnected power system with proper tie line connections has been illustrated in Figure 1(c). The inner structure of any particular area can be related to Figure 1(a) for more detailed insight. The LFC loop maintains the system frequency to the rated value in an IPS. Appendix A contains a list of the time constant, gain, and other system parameters of the under-investigation IPS, which have been taken from [38]. The gas speed regulation(R_g), hydrospeed regulation (R_h), wind speed regulation (R_w), thermal reheat speed regulation (R_t), and ith area's bias factor (B_i) are all included in the LFC loop of the area: controller ($K_{LFC}(s)$), and generator/load ($\frac{K_{p(i)}}{sT_{p(i)}+1}$). The thermal reheat unit consists of a thermal governor ($\frac{1}{sT_{gr}+1}$), reheat turbine ($\frac{K_{re}T_{re}}{sT_{re}+1}$), and thermal turbine ($\frac{1}{sT_{tr}+1}$); the hydro unit consists of transient droop compensation ($\frac{sT_{rs}+1}{sT_{rh}+1}$), hydro governor ($\frac{1}{sT_h+1}$), and hydro turbine ($\frac{1-sT_w}{1+0.5T_w s}$); the gas unit comprises a gas governor ($\frac{Xs+1}{Ys+1}$), valve position ($\frac{a}{bs+c}$), fuel system ($\frac{1-sT_{CR}}{1+sT_f}$), and compressor discharge system ($\frac{1}{sT_{CD}+1}$); the wind unit consists of data fit pitch response and hydraulic pitch actuator blocks; the solar photovoltaic system consists of a straight step function. $\Delta P_{D(i)}$, $\Delta P_{tie(i)}$, $\Delta V_{t(i)}$, and denote the deviations in load, tie-line power, terminal voltage, and load frequency, respectively. $V_{s(i)}$, and $V_{t(i)}$ depict the sensor, reference, error, and terminal voltage in the ith area, respectively. The AVR loop of the ith area comprises an amplifier ($\frac{K_{a(i)}}{sT_{a(i)}+1}$), generator ($\frac{K_{g(i)}}{sT_{g(i)}+1}$), exciter ($\frac{K_{e(i)}}{sT_{e(i)}+1}$), sensor ($\frac{K_{s(i)}}{sT_{s(i)}+1}$), and controller ($K_{AVR}(s)$). To couple AVR and LFC loops, different coupling coefficients are used, including K_1, K_2, K_3, K_4, and P_s. T_{ij} denotes

TABLE 2. Literature summary.

Reference of Paper	Area of Research	Tuning Method	Suggested Controller	Generation Sources	Year	Generation Sources in all Areas	Covered Area	Additional Incorporation for Improvements	Nonlinearities
[1]	LFC and AVR	AOA, LPBO, MPSO	PI-PD	-	2022	2,3	2, 3	-	-
[2]	LFC and AVR	DO	PI-PD	Reheat thermal, Hydro, and Gas	2022	6	2, 3	-	GDB, BD, GRC
[3]	LFC and AVR	SA, ZN	PID	Hydro and Nonreheat thermal	2016	4	2	-	GDB
[4]	LFC and AVR	NN-FTF	Hybrid NN and FTF	-	2016	1	1	-	-
[5]	LFC and AVR	ZN, FLC	PID, Fuzzy	-	2018	1	1	-	-
[6]	LFC and AVR	LSA	PIDF, PID^{u}F	Reheat thermal, Wind, and Diesel	2018	4	2	IPFC, SMES	GDB, GRC
[7]	LFC and AVR	MFO	FOOD	Hydro and Nonreheat thermal	2019	4	2	-	GDB, BD
[8]	LFC and AVR	FA	PID	Hydro and Nonreheat thermal	2019	4	2	-	-
[9]	LFC and AVR	IPSO	CPSS	Gas, Reheat thermal, and Hydro	2020	1	1	-	GDB, GRC
[10]	LFC and AVR	DE-AEFA	PID	Wind, Hydro, Thermal, Gas, Solar, and Diesel	2020	6	2	HVDC link	GRC
[11]	LFC and AVR	DE-AEFA	PID	Gas, Diesel, Hydro, Solar photovoltaic, Reheat thermal, and Wind	2020	6	2	IPFC, RFBs	GRC
[12]	LFC and AVR	SCA	PIDF, PI	Reheat thermal and Nonreheat thermal	2020	2	2	UPFC, RFBs	-
[13]	LFC and AVR	NLTA	PID	-	2021	2	2	-	-
[14]	LFC and AVR	GWO	PIDD	Reheat thermal, Hydro, and Nuclear	2021	6	2	SMES, UPFC	GRC, GDB
[15]	LFC and AVR	FA	PID	Reheat thermal and Hydro	2021	4	2	-	TD, GRC, GDB
[16]	LFC and AVR	hFPAPFA	PIDA	Thermal	2021	1	1	-	-
[17]	LFC and AVR	HHO	TIDF	Reheat thermal and Combined cycle gas turbine (CCGT)	2021	6	3	-	GDB, GRC, BD
[18]	LFC and AVR	2nd order error-driven control law	ADRC	Solar, Geothermal, Wind, and EVs	2022	6	3	-	-
[19]	LFC and AVR	HHO	2DOF I-TDF	Reheat thermal, Wind, Solar thermal, and Dish-Stirling,	2022	6	3	-	GDB, GRC
[20]	LFC and AVR	AFA	CFPD-TID	Hydro, Thermal, and Geothermal	2022	6	3	RFBs, HVDC link	GRC, DB
[21]	LFC and AVR	AFA	CFOTDN-FOPDN	Hydro, Dish-Stirling, Solar thermal, and Reheat thermal	2022	4	2	-	GDB, CTD, GRC
[22]	LFC and AVR	AFA	CPDN-FOPIDN	Reheat thermal, Hydro, Gas, and Geothermal	2022	6	3	FESS, CES, RFBs, SMES HVDC link	GRC, GDB
[23]	LFC and AVR	DPO	PIDA	Three Bioenergy technologies and Two solar energy sources	2022	10	2	-	-
[24]	LFC and AVR	HAEFA	Fuzzy PID	Reheat thermal, Hydro, and Gas	2022	6	2	UCs, SMES, RFBs	-
[25]	LFC and AVR	GBO	FPIDD^{2}	Thermal, gas, hydraulic, wind, and solar power	2023	8	2	-	GRC, GDB, CTD
[26]	LFC	ICA	FTIλDN	Reheat thermal	2021	2,5	2,5	MFs	GRC, GDB
[38]	LFC and AVR	GBO	PID	Thermal, Gas, Hydro, Wind, and Solar	2023	20	4	-	-
Proposed Method	LFC and AVR	OOBO	PI-PD	Thermal, Gas, Hydro, Wind, and Solar	2024	20	4	-	GRC, GDB, BD

the coefficient of synchronization between the ith and ith areas. The transfer function of the gas ($G_G(s)$), reheat thermal ($G_T(s)$), hydro ($G_H(s)$), wind ($G_W(s)$), and solar photovoltaic ($G_S(s)$) systems are provided in Eq. (1)–(5), respectively [38]. Table 1 defines the terms used in the LFC and AVR systems.

$$G_G(s) = \frac{(1+Xs)(1-T_{CR}s)a}{(1+Ys)(c+bs)(1+T_F s)(1+T_{CD}s)} \quad (1)$$

$$G_T(s) = \frac{1+T_{re}K_{re}s}{(1+T_{gr}s)(1+T_{re}s)(1+T_{tr}s)} \quad (2)$$

$$G_H(s) = \frac{(1+T_{rs}s)(1-T_w s)}{(1+T_h s)(1+T_{rh}s)(1+0.5T_w s)} \quad (3)$$

$$G_W(s) = \frac{K_{w1}K_{w2}(1+T_{w1}s)}{(1+T_{w2}s)(s^2+2s+1)} \quad (4)$$

$$G_S(s) = \frac{K_{pv}}{1+T_{pv}} \quad (5)$$

The voltage of the synchronous generator is regulated to a predetermined level with the aid of an AVR loop. The error voltage is determined by continuously comparing the output voltage with the reference signal. Before the error signal is fed to the exciter to change the excitation of the generator field, it is amplified. This process stabilizes the system and immediately eliminates fluctuations in the terminal voltage.

Different linearities have been included in thermal reheat and hydropower plants such as generation rate constraints (GRC), generator dead band (GDB), and boiler dynamics (BD). These nonlinearities have been included to make the system make real sense. These nonlinearities have been briefed below.

A. GENERATION RATE CONSTRAINT (GRC)

The main sources of GRC in the steam turbine are both mechanical and thermodynamic constraints. Saturation nonlinearity, which imposes significant constraints on the steam turbine, is the cause of GRC. This constraint must be considered when modeling the power plant, otherwise, there is a risk of exposing the system to extreme turbulence, which can lead to governor wear [2]. The GRC is often lower for thermal power plants than for hydropower plants. The GRC for hydropower plants is 270%/min for higher generation and 360%/min for lower generation. The GRC for thermal power plants with reheat has an upper limit of 3%/min [47].

B. GOVERNOR DEAD BAND (GDB)

GDB is a measure of the total steady state velocity variations, that do not change the governor valve. The GDB, which is always specified as a percentage of the rated speed, shows how insensitive the speed control system is [2]. The backlash form of non-linearity is used to specify the GDB. The GDB value for hydropower plants is set at ±0.02 %, while the GDB value for thermal reheat plants can be computed using Eq. (6) [47].

$$\text{GDB} = \frac{-0.0637\text{s} + 0.8}{\text{s} + 1} \quad (6)$$

C. BOILER DYNAMICS (BD)

The combustion control is incorporated into the boiler dynamics transfer function model, as shown in Figure 2. This model can be used to analyze a variety of plants, e.g. those fired with coal and having precisely controlled combustion, and those fired with gas or oil and having inadequate combustion control. In most steam power plants, turbine control valves are used to effect changes in generation. When fluctuations in pressure and steam flow are detected, the boiler control system quickly makes the necessary adjustments. The transfer function for boiler dynamics is shown in Figure 2 [2].

III. PROPOSED CONTROL STRATEGY

Figure 3 shows the proposed control strategy to control the LFC and AVR control loops of four-area multi-source IPS. PI-PD controller has been used for the effective control of terminal voltage and load frequency. R(s), Y(s), U(s) and E(s) represent reference, output, control, and error signals, respectively. PI-PD is an improved version of the conventional PID controller [1], [2]. It has proportional & integral terms (PI) in the feedforward path and proportional & derivative terms (PD) in the feedback path of the closed-loop system to provide optimal stability and control. K_{p1}, K_i, K_{p2}, and K_d are gains of the PI-PD controller. The control signal ($U_{PI-PD}(s)$) for the PI-PD controller can be expressed using Eq. (7) [1], [2].

$$U_{PI-PD}(s) = (K_{p1} + \frac{K_i}{s})E(s) - (K_{p2} + K_d s)Y(s) \quad (7)$$

where Y(s) represents the output of the system.

Moreover, I-P, PID, and I-PD schemes have also been explored for a comprehensive comparative analysis. The structure of PID, I-P, and I-PD controllers have been presented in Figures 4(a), 4(b), and 4(c) respectively. The industrial sector makes substantial use of the classic PID controller because of its enduring traits of great operating efficiency and simple design. In the PID controller, proportional, integrator & derivative terms are located in the feedforward path of the closed-loop system. K_p, K_i, and K_d are gains of the PID controller. The control signal ($U_{PID}(s)$) for the PID controller can be expressed using Eq. (8) [38].

$$U_{PID}(s) = (K_p + \frac{K_i}{s} + K_d s)E(s) \quad (8)$$

I-PD controller is also a modified form of PID controller in which, the integral term is placed in the feedforward direction, whereas the proportional and derivative terms are situated in the feedback path of a closed-loop system. K_i, K_p, and K_d are gains of the I-PD controller. The control signal ($U_{I-PD}(s)$) for the I-PD controller can be expressed using Eq. (9) [38].

$$U_{I-PD}(s) = (\frac{K_i}{s})E(s) - (K_p + K_d s)Y(s) \quad (9)$$

In the I-P controller, proportional and integral terms are positioned in the feedback and feedforward paths respectively. K_i and K_p are gains of the I-P controller. The control

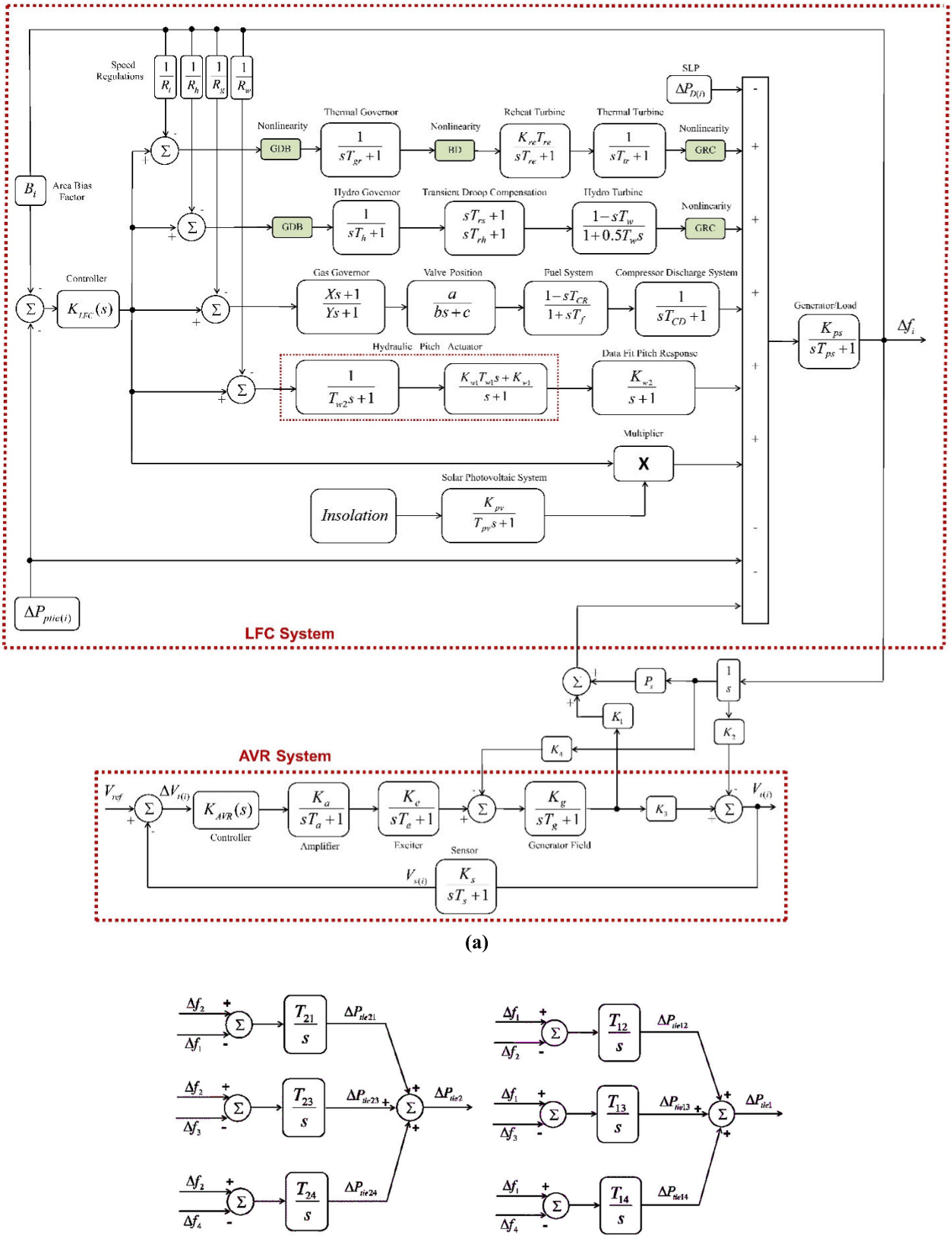

(a)

FIGURE 1. Generalized IPS Model (b) Tie-line connections (c) Combined model of Four-Area IPS [38].

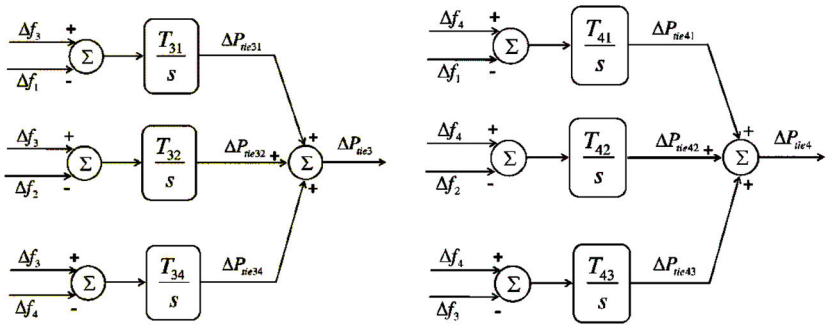

(b)

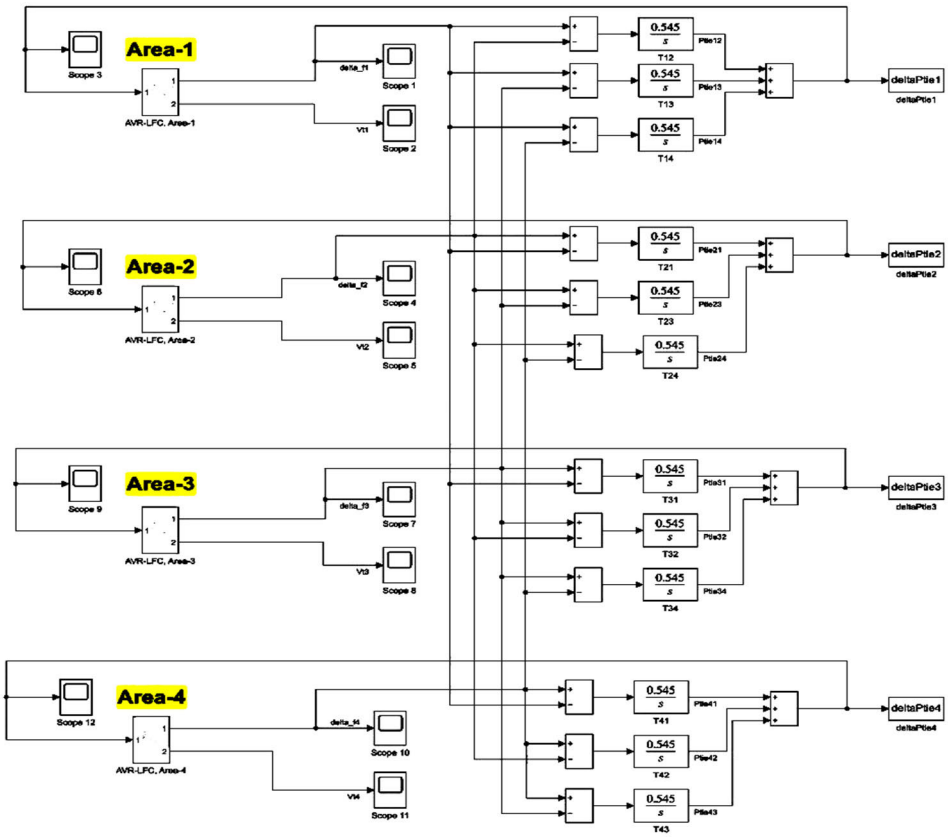

(c)

FIGURE 1. *(Continued.)* **Generalized IPS Model (b) Tie-line connections (c) Combined model of Four-Area IPS [38].**

signal ($U_{I-P}(s)$) for the I-P controller can be expressed using Eq. (10) [38].

$$U_{I-P}(s) = (\frac{K_i}{s})E(s) - (K_p)Y(s) \tag{10}$$

The cost function (J) is optimized (minimized) to determine the ideal controller parameters of the PI-PD with OOBO. The integral of time multiplied by the squared value of the error (ITSE) was used as the error index to obtain the optimal controller parameters. In this work, the cost function (J) was minimized using OOBO. For a combined control of terminal voltage and load frequency, J can be expressed with ITSE using Eq. (11) [38]:

$$\text{JITSE} = \int_0^T t[\Delta f^2 + \Delta V_t^2 + \Delta P_{tie}^2]dt \tag{11}$$

where

$$\Delta f^2 = \Delta f_1^2 + \Delta f_2^2 + \Delta f_3^2 + \Delta f_4^2 \tag{12}$$

$$\Delta V_t^2 = \Delta V_{t1}^2 + \Delta V_{t2}^2 + \Delta V_{t3}^2 + \Delta V_{t4}^2 \tag{13}$$

$$\Delta P_{tie}^2 = \Delta P_{tie1}^2 + \Delta P_{tie2}^2 + \Delta P_{tie3}^2 + \Delta P_{tie4}^2 \tag{14}$$

$$\Delta V_{t1} = V_{ref} - V_{t1} \tag{15}$$

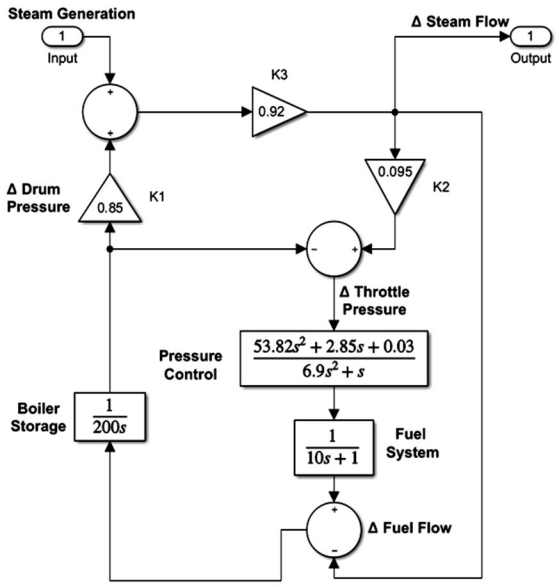

FIGURE 2. Transfer function model boiler dynamics [2].

$$\Delta V_{t2} = V_{ref} - V_{t2} \quad (16)$$
$$\Delta V_{t3} = V_{ref} - V_{t3} \quad (17)$$
$$\Delta V_{t4} = V_{ref} - V_{t4} \quad (18)$$
$$\Delta P_{ptie1} = \Delta P_{ptie12} + \Delta P_{ptie13} + \Delta P_{ptie14} \quad (19)$$
$$\Delta P_{ptie2} = \Delta P_{ptie21} + \Delta P_{ptie23} + \Delta P_{ptie24} \quad (20)$$
$$\Delta P_{ptie3} = \Delta P_{ptie31} + \Delta P_{ptie32} + \Delta P_{ptie34} \quad (21)$$
$$\Delta P_{ptie4} = \Delta P_{ptie41} + \Delta P_{ptie42} + \Delta P_{ptie43} \quad (22)$$

A. ONE-TO-ONE BASED OPTIMIZER (OOBO)

This section covers the details of the optimization algorithm OOBO. It is a meta-heuristic algorithm that is capable of providing an optimal and speedy solution to the optimization problem in an iterative way. OOBO was discovered in 2023 by Dehghani [48]. It utilizes the population search power in the problem-solving space. The Flow Chart for OOBO is given in Figure 5.

1) OOBO FUNDAMENTALS

OOBO optimizes the problem in several steps. First of all, multiple possible solutions are generated that relate to the problem constraints. In the next step, the main idea is implemented where the position of each generated solution is updated in the search space in each iteration. OOBO algorithm differs from traditional and contemporary optimization algorithms in a way that it does not rely heavily on a specific number of search spaces. It does not use the traditional way of taking a specific number of solutions and updating them to find an optimal solution that mistakenly leads to the local optimal areas. OOBO works by involving all the members of the search space in the update process and places each solution in its new position in a one-to-one-based approach. The following factors are included in the updation process.

a. All members of the population are considered rather than focusing on the selected population
b. Inclusion of all the members in the process of update
c. Each solution is placed in one-to-one correspondence.

2) OOBO INITIALIZATION

In OOBO, all the members in the search space are taken as the solution to the problem. These solutions are taken as values of the decision variables. The values rely on the position of these members in the search space. Mathematically, each member of the OOBO is represented as a vector. The number of elements of the vector is the same as the number of decision variables in OOBO. A member of the population can be represented mathematically as

$$\overrightarrow{X}_i = [x_{i,1}, \ldots\ldots, x_{i,d}, \ldots.., x_{i,m}], \quad i = 1, \ldots.., N \quad (23)$$

The members of the population in OOBO are placed randomly to generate the population in the initial stage. The random positioning is performed using the relation:

$$x_{i,d} = lb_d + rand().(ub_d - lb_d), \quad d = 1, \ldots\ldots, m \quad (24)$$

where represents ith population member, $x_{i,d}$ shows dth dimension, rand() is a random function generator in the interval of [0,1] and N is the size of the population. The population members in OOBO are shown in a matrix form as

$$\overrightarrow{X} = \begin{bmatrix} \overrightarrow{X_1} \\ \vdots \\ \overrightarrow{X_i} \\ \vdots \\ \overrightarrow{X_N} \end{bmatrix} = \begin{bmatrix} x_{1,1} & \cdots & x_{1,d} & \cdots & x_{1,m} \\ \vdots & \ddots & \vdots & \vdots & \vdots \\ x_{i,1} & \cdots & x_{i,d} & \cdots & x_{i,m} \\ \vdots & \vdots & \vdots & \ddots & \vdots \\ x_{N,1} & \cdots & x_{N,d} & \cdots & x_{N,m} \end{bmatrix} \quad (25)$$

Since each member of the population is also a proposed solution, the objective function is evaluated based on each member of the population. This gives different values of the objective function at each iteration. The number of values of the objective function is equal to the size of the population. The objective function can be expressed as

$$\overrightarrow{F} = \begin{bmatrix} f_1 \\ \vdots \\ f_i \\ \vdots \\ f_N \end{bmatrix}_{N\times 1} = \begin{bmatrix} f(\overrightarrow{X_1}) \\ \vdots \\ f(\overrightarrow{X_i}) \\ \vdots \\ f(\overrightarrow{X_N}) \end{bmatrix}_{N\times 1} \quad (26)$$

where is the vector of the objective function and is the objective function's values.

3) MATHEMATICAL MODELING OF OOBO

The mathematical modeling of OOBO is heavily based on its main idea. OOBO prevents the way of updating the position of the solution in each iteration as used by the other algorithms. Most of the algorithms choose the selected proposed

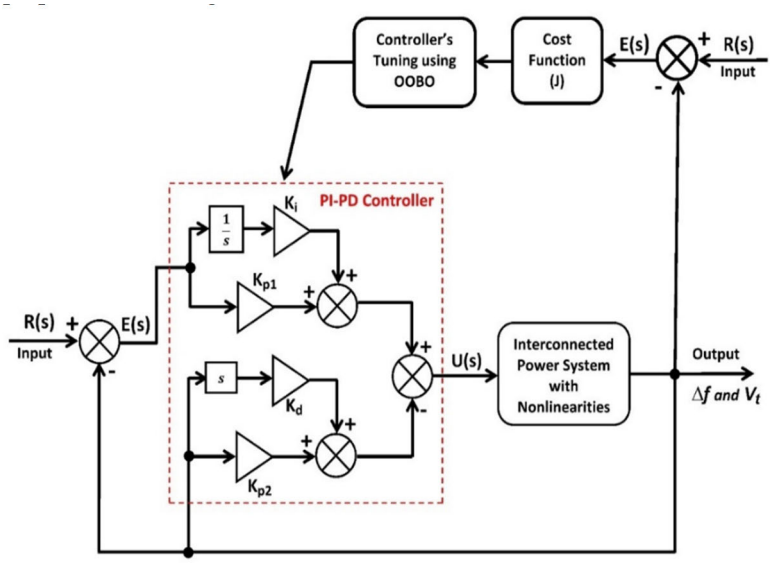

FIGURE 3. Proposed Control strategy using PI-PD [1], [2].

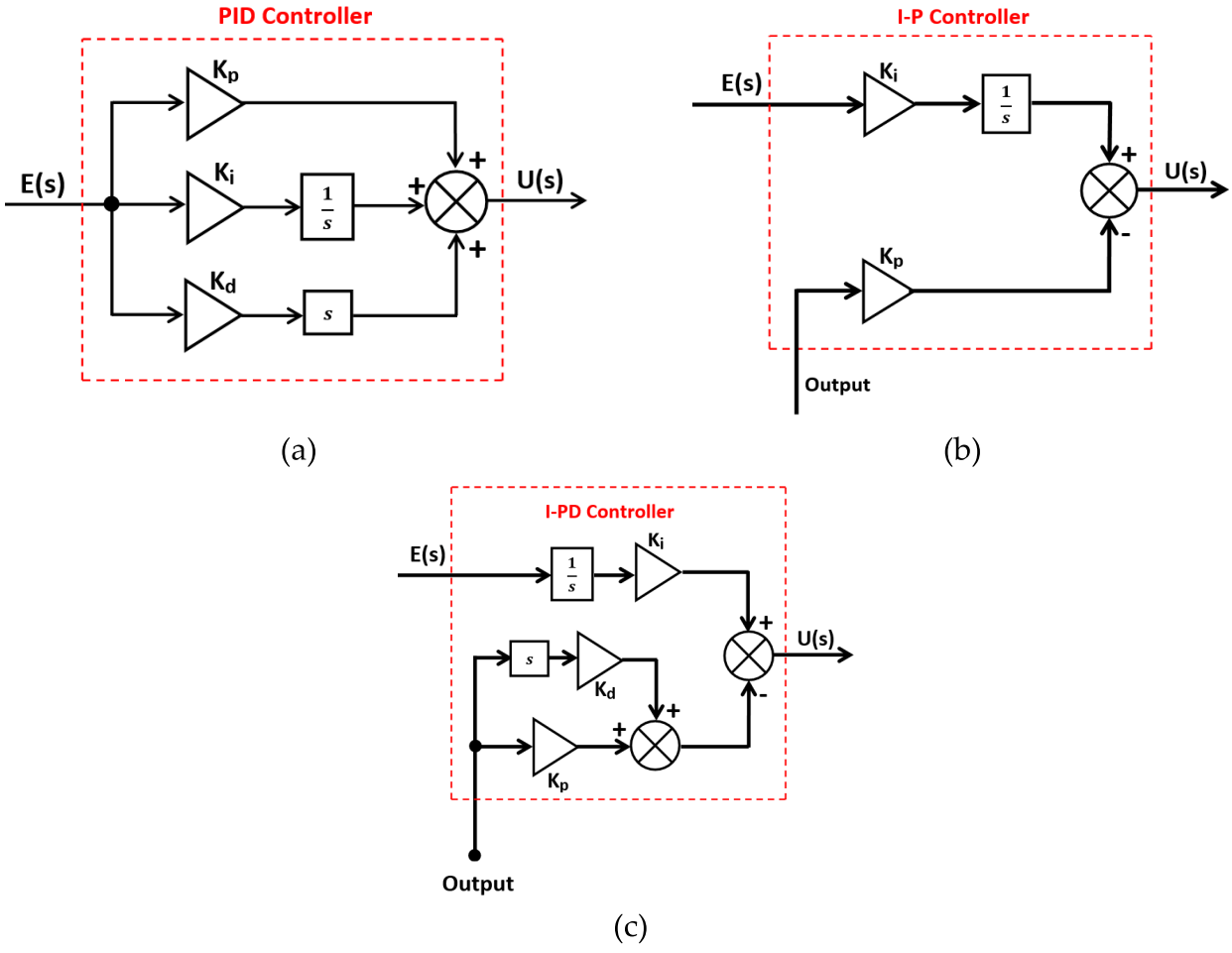

FIGURE 4. (a) PID Controller (b) I-P Controller (c) I-PD Controller [38].

solutions as their best members and apply the process of updating in each iteration. This process leads to the local optimum values and is not a good solution. This also creates a problem in finding the global optimum values for a complex

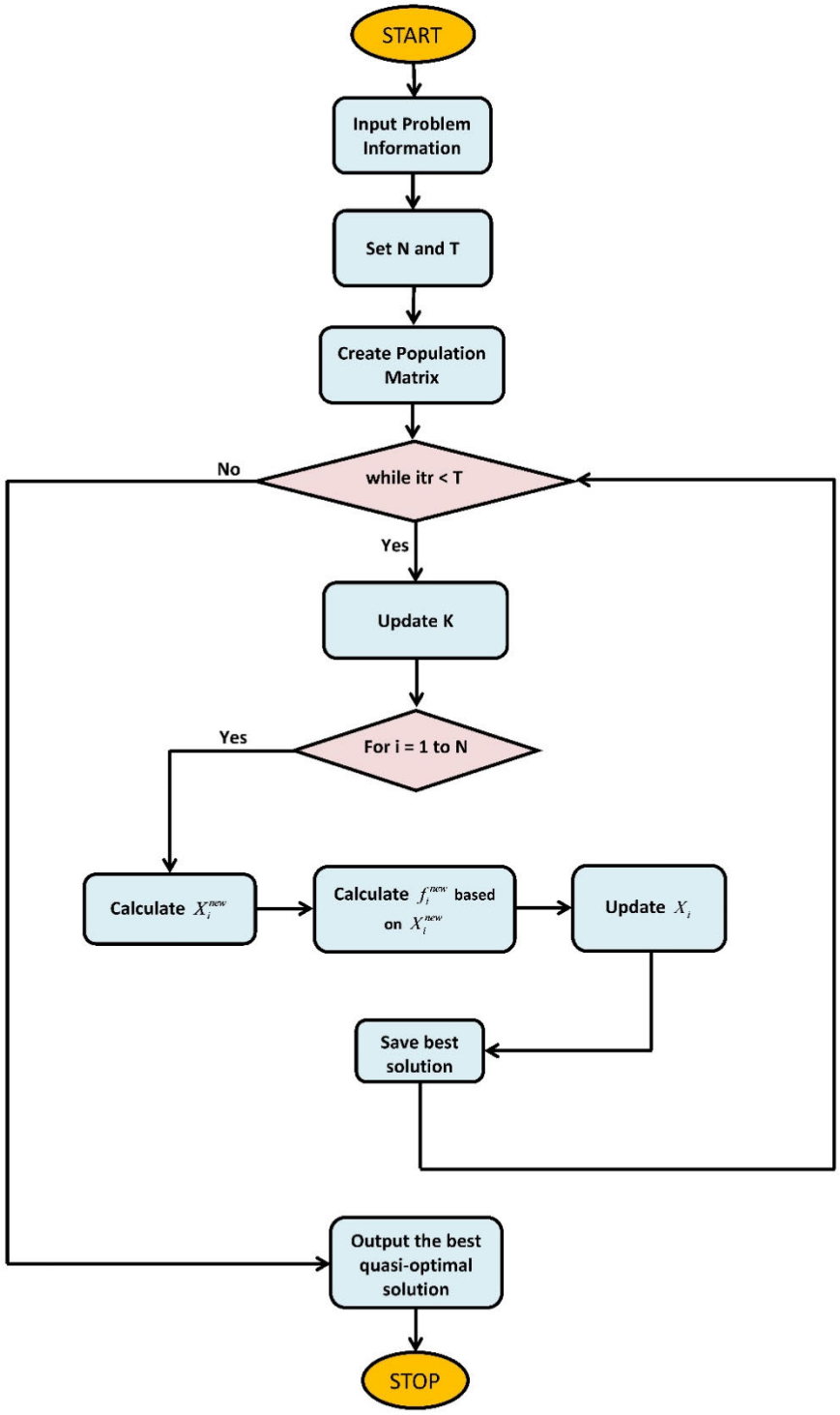

FIGURE 5. Flow Chart for OOBO [48].

optimization problem. OOBO works differently by moving the population of the algorithm in different search spaces. This increases the capability of the algorithm to explore new areas and find solutions to a global search. This is performed by involving each population member in the update process. The method selects one member at a time from the population randomly and it guides another member of the population in the search space. This idea can be mathematically expressed as an N-tuple having characteristics such as a) each member from the population is selected randomly from positive integers 1 to N. b) There is no duplicate member in the whole population c) the value of the member is not equal

TABLE 3. Optimum controller parameters.

Area	OOBO−PID		OOBO−I-P		OOBO−I-PD		OOBO−PI-PD	
	Controller Parameter	Value	Controller Parameter	Value	Controller Parameter	Value	Controller Parameter	Value
Area−1	K_{p1}	1.0156	K_{i1}	1.7932	K_{i1}	0.1205	K_{p1}	1.4358
	K_{i1}	1.0705	K_{p1}	0.5424	K_{p1}	1.1693	K_{i1}	0.4906
	K_{d1}	1.3475	K_{i2}	0.5695	K_{d1}	1.5098	K_{p2}	0.0124
	K_{p2}	1.9402	K_{p2}	0.3291	K_{i2}	0.9247	K_{d1}	1.1564
	K_{i2}	2	-	-	K_{p2}	0.7901	K_{p3}	0.8687
	K_{d2}	1.4379	-	-	K_{d2}	1.6420	K_{i2}	1.3462
	-	-	-	-	-	-	K_{p4}	0.7540
	-	-	-	-	-	-	K_{d2}	0.6899
Area−2	K_{p3}	0.5701	K_{i3}	0.3537	K_{i3}	1.3866	K_{p5}	1.2331
	K_{i3}	0.7678	K_{p3}	1.1088	K_{p3}	0.3926	K_{i3}	0.4503
	K_{d3}	2	K_{i4}	0.8985	K_{d3}	0.5067	K_{p6}	1.2045
	K_{p4}	1.0287	K_{p4}	0.6106	K_{i4}	0.7381	K_{d3}	1.6231
	K_{i4}	1.9336	-	-	K_{p4}	0.6757	K_{p7}	1.6617
	K_{d4}	1.6063	-	-	K_{d4}	0.1501	K_{i4}	1.9456
	-	-	-	-	-	-	K_{p8}	1.1736
	-	-	-	-	-	-	K_{d4}	1.3570
Area−3	K_{p5}	0.0100	K_{i5}	0.9827	K_{i5}	0.5214	K_{p9}	1.1088
	K_{i5}	1.6285	K_{p5}	1.2244	K_{p5}	1.7813	K_{i5}	1.7442
	K_{d5}	0.8517	K_{i6}	0.4460	K_{d5}	0.7722	K_{p10}	1.9905
	K_{p6}	2	K_{p6}	0.6212	K_{i6}	1.4664	K_{d5}	0.7195
	K_{i6}	0.9814	-	-	K_{p6}	1.4837	K_{p11}	1.1221
	K_{d6}	1.7461	-	-	K_{d6}	1.2872	K_{i6}	0.9642
	-	-	-	-	-	-	K_{p12}	0.2401
	-	-	-	-	-	-	K_{d6}	0.0432
Area−4	K_{p7}	2	K_{i7}	0.9465	K_{i7}	1.0093	K_{p13}	0.3982
	K_{i7}	0.8711	K_{p7}	0.6799	K_{p7}	1.3343	K_{i7}	0.7595
	K_{d7}	1.0537	K_{i8}	1.5021	K_{d7}	1.7173	K_{p14}	1.4071
	K_{p8}	1.1733	K_{p8}	1.5818	K_{i8}	0.5889	K_{d7}	0.9323
	K_{i8}	0.4791	-	-	K_{p8}	0.8491	K_{p15}	1.4569
	K_{d8}	0.9877	-	-	K_{d8}	0.2259	K_{i8}	1.6843
	-	-	-	-	-	-	K_{p16}	1.2823
	-	-	-	-	-	-	K_{d8}	1.2518
	ITSE		ITSE		ITSE		ITSE	

to its position in the N-tuple. The mathematical model of the OOBO represents the one-to-one correspondence as the position number of the population members in the search space. The member position is used in the population matrix. The set K comprising the position numbers of the guiding members is expressed as

$$\overrightarrow{K} = \{[k_1, \ldots . k_{\updownarrow}, \ldots . . k_N] \in P_{\overline{N}}; \forall \updownarrow \in \overline{N} : k_{\updownarrow} \neq \updownarrow\} \quad (27)$$

where $N = \{1 \ldots . N\}$, $P_{\overline{N}}$ is the set of all permutations, of set N and $k_{\updownarrow}$ is the $^{\updownarrow}$th element of vector K. The update process of OOBO works in a way; to guide the ith member in the population matrix Xi, a position member Xki is selected from the population matrix. Then the objective function values of both the numbers are taken and checked. If the values show the status of Xki is better than Xi, Xi will move to the position of Xki, otherwise it will move away from Xki. This process

TABLE 4. Numerical results for LFC loops.

Control Strategy	Area-1				Area-2			
	Settling Time	% Overshoot	Undershoot	% s-s Error	Settling Time	% Overshoot	Undershoot	% s-s Error
OOBO-PID	8.24	0.36	-0.65	0	8.23	0.38	-0.61	0
OOBO-I-P	13.40	0.04	-0.15	0	10.9	0.009	-0.12	0
OOBO-I-PD	26.11	0.02	-0.053	0	28.47	0.054	-0.091	0
OOBO-PI-PD	19.18	0.008	-0.091	0	19.67	0.005	-0.068	0
Control Strategy	Area-3				Area-4			
	Settling Time	% Overshoot	Undershoot	% s-s Error	Settling Time	% Overshoot	Undershoot	% s-s Error
OOBO-PID	8.24	0.39	-0.65	0	8.21	0.36	-0.7	0
OOBO-I-P	15.65	0.006	-0.088	0	15.18	0.03	-0.12	0
OOBO-I-PD	28.80	0.015	-0.045	0	29.74	0.013	-0.052	0
OOBO-PI-PD	19.36	0.0048	-0.087	0	21.11	0.0049	-0.057	0

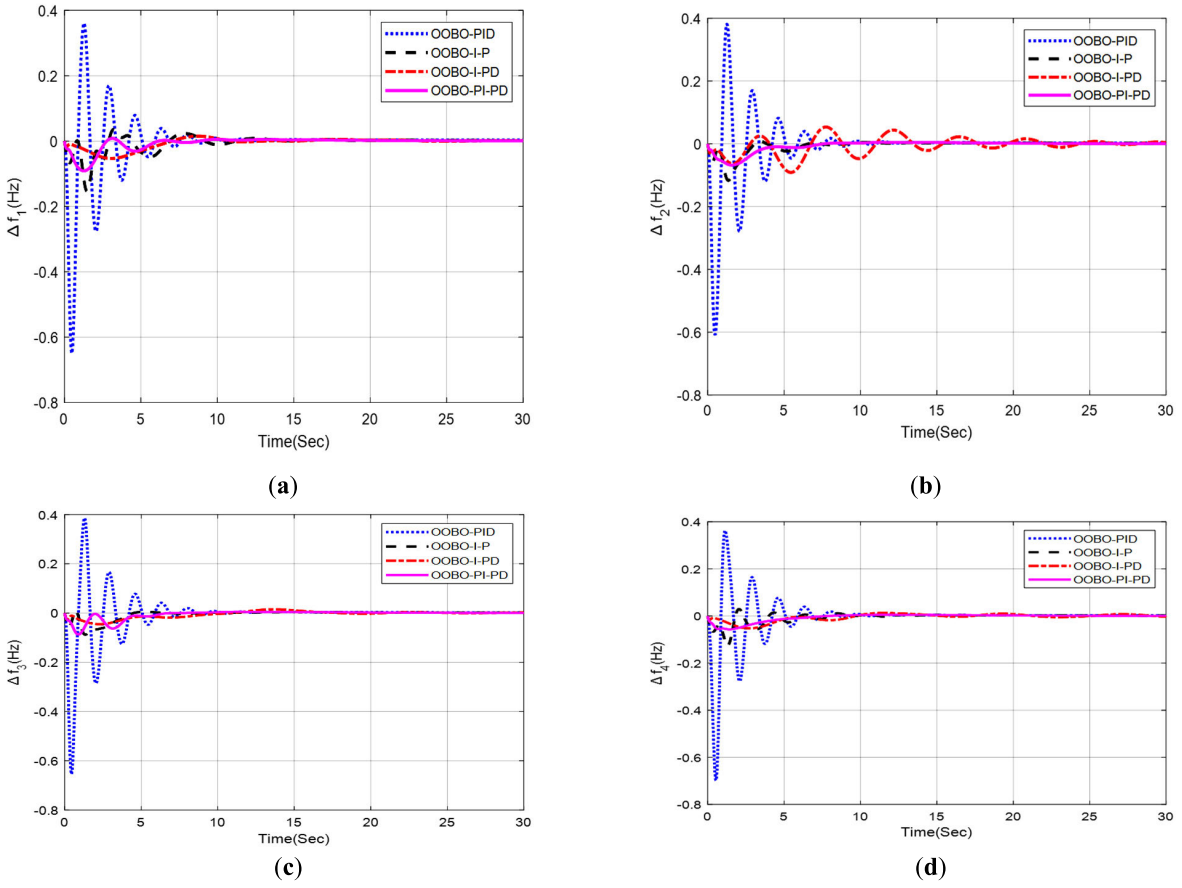

FIGURE 6. LFC responses: (a)Δf1; (b)Δf2; (c)Δf3; (d)Δf4.

is used to model the new position of the population members in the search space. This is expressed as

$$x_{i,d}^{new} = \begin{cases} x_{i,d} + rand().(x_{ki,d} - Ix_{i,d}), & f_{ki} < f_i \\ x_{i,d} + rand().(x_{i,d} - x_{ki,d}), & otherwise \end{cases} \quad (28)$$

$$I = round(1 + rand()) \quad (29)$$

where $x_{i,d}^{new}$ is the newly updated position of the ith member in the dth dimension. $x_{ki,d}$ represents the dth dimension of the selected member to guide ith member. I have values from the

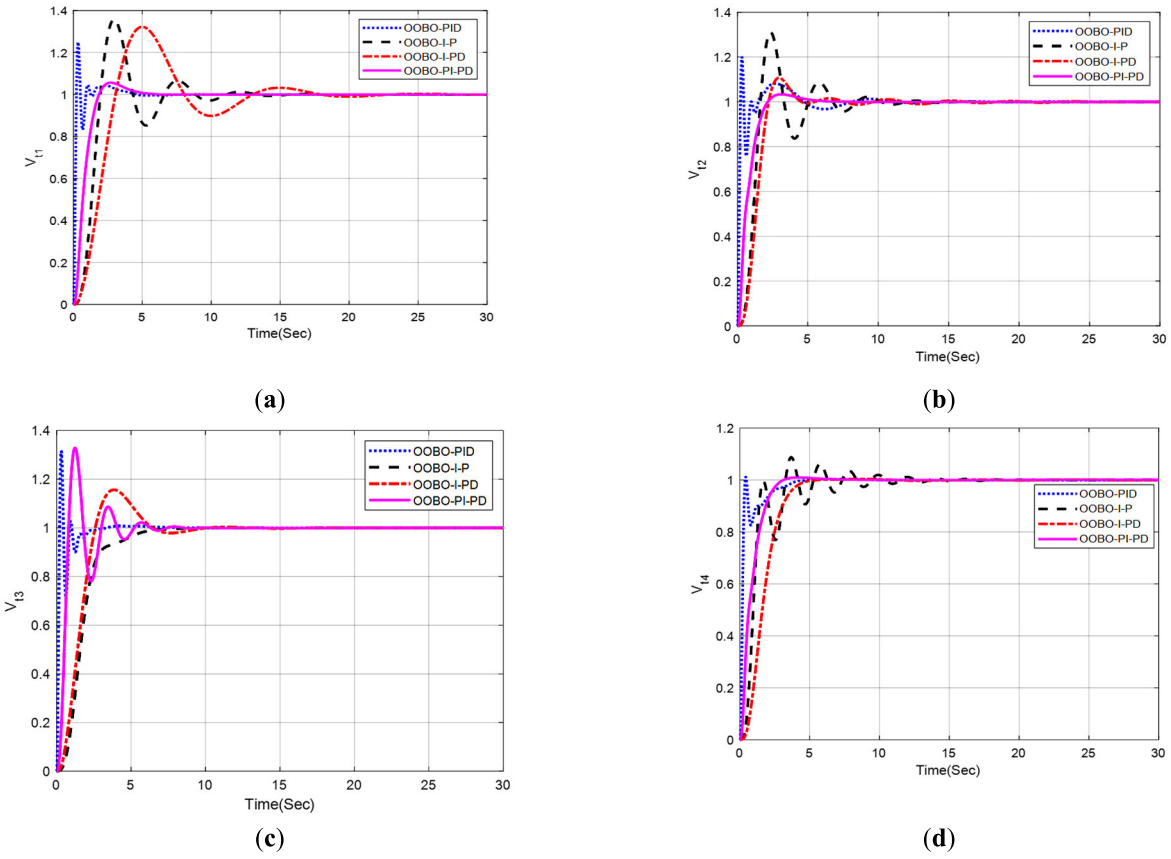

FIGURE 7. AVR responses:(a) Vt1; (b) Vt2; (c) Vt3; (d) Vt4.

TABLE 5. Numerical results for AVR loops.

Control Strategy	Area-1			Area-2		
	Settling Time	% Overshoot	% s-s Error	Settling Time	% Overshoot	% s-s Error
OOBO-PID	3.35	24.91	0	7.13	20.01	0
OOBO-I-P	10.43	35.71	0	9.50	31.07	0
OOBO-I-PD	16.52	32.35	0	4.18	10.83	0
OOBO-PI-PD	4.21	5.61	0	4.28	3.35	0
Control Strategy	Area-3			Area-4		
	Settling Time	% Overshoot	% s-s Error	Settling Time	% Overshoot	% s-s Error
OOBO-PID	2.07	31.64	0	3.42	1.27	0
OOBO-I-P	5.61	0	0	9.11	8.73	0
OOBO-I-PD	8.01	15.68	0	4.15	0.44	0
OOBO-PI-PD	5.84	32.87	0	2.62	0.93	0

set $\{1,2\}$. f_{ki} is the value of the object function that is based on Xki The basic principle of the update process is that the new status of the member is acceptable only if it is better than the previous status otherwise it will remain at the same position as before. This is represented mathematically as,

$$X_i = \begin{cases} X_i^{new}, & f_i^{new} < f_i \\ X_i, & otherwise \end{cases} \tag{30}$$

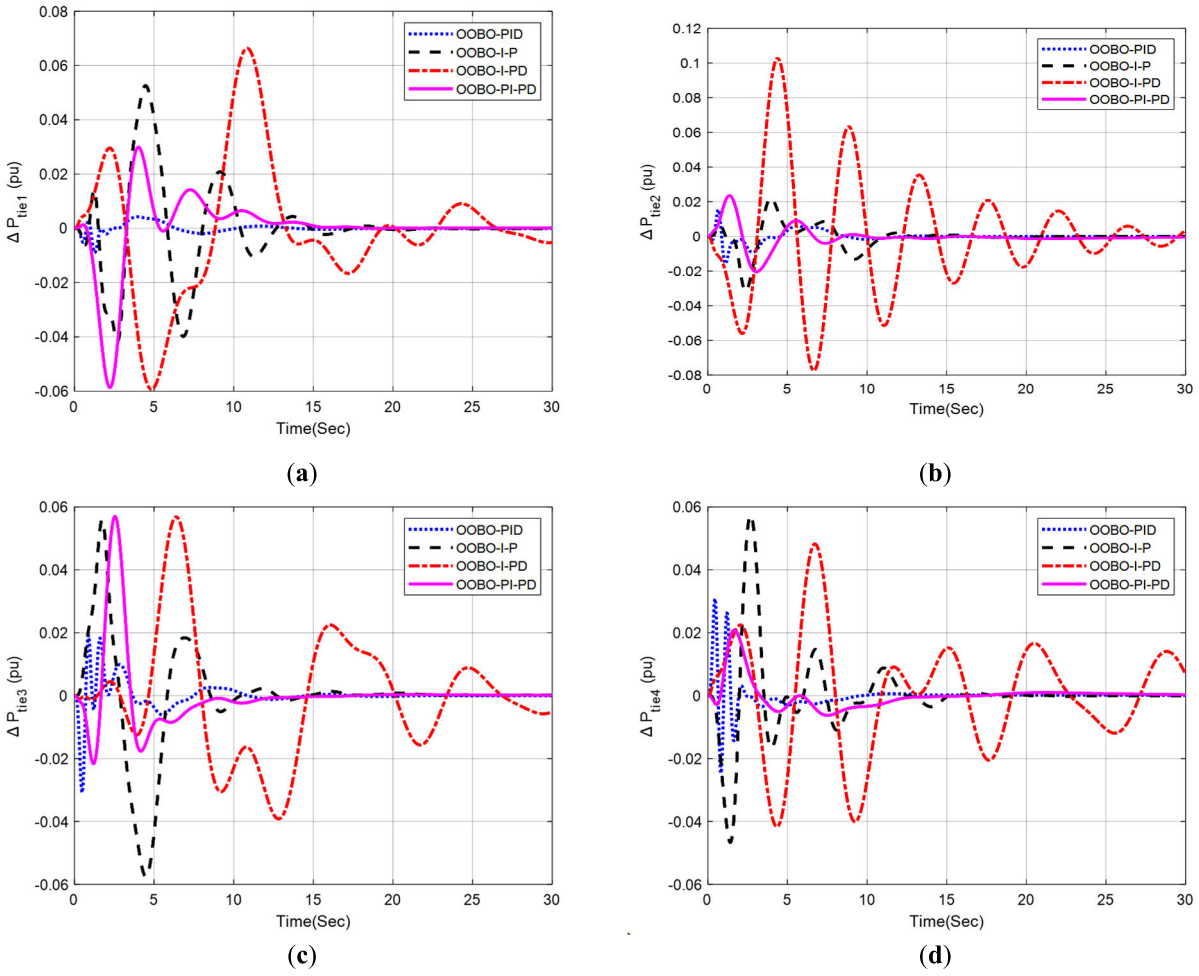

FIGURE 8. Tie-line power deviation responses: (a)ΔPtie1; (b)ΔPtie2; (c)ΔPtie3; (d)ΔPtie4.

TABLE 6. Numerical results of tie-line power deviations.

Control Strategy	Area-1			Area-2		
	Settling Time	% Overshoot	Undershoot	Settling Time	% Overshoot	%Undershoot
OOBO-PID	17.02	0.004	-0.009	11.93	0.015	-0.016
OOBO-I-P	16.77	0.053	-0.04	19.6	0.022	-0.032
OOBO-I-PD	28.72	0.07	-0.0590	29.73	0.10	-0.077
OOBO-PI-PD	14.74	0.03	-0.0587	25.4	0.024	-0.020
Control Strategy	**Area-3**			**Area-4**		
	Settling Time	**% Overshoot**	**Undershoot**	**Settling Time**	**% Overshoot**	**% Undershoot**
OOBO-PID	13.59	0.019	-0.031	9	0.031	-0.025
OOBO-I-P	16.4	0.056	-0.058	14.8	0.057	-0.047
OOBO-I-PD	28.2	0.057	-0.039	29.90	0.048	-0.042
OOBO-PI-PD	11.8	0.057	-0.022	24.37	0.021	-0.0063

where represents the updated status of ith member in the population while representing its objective function values.

4) PSEUDOCODE AND FLOW CHART OF OOBO

After the first update step, the process goes on repeatedly based on the updated status of the members. At each

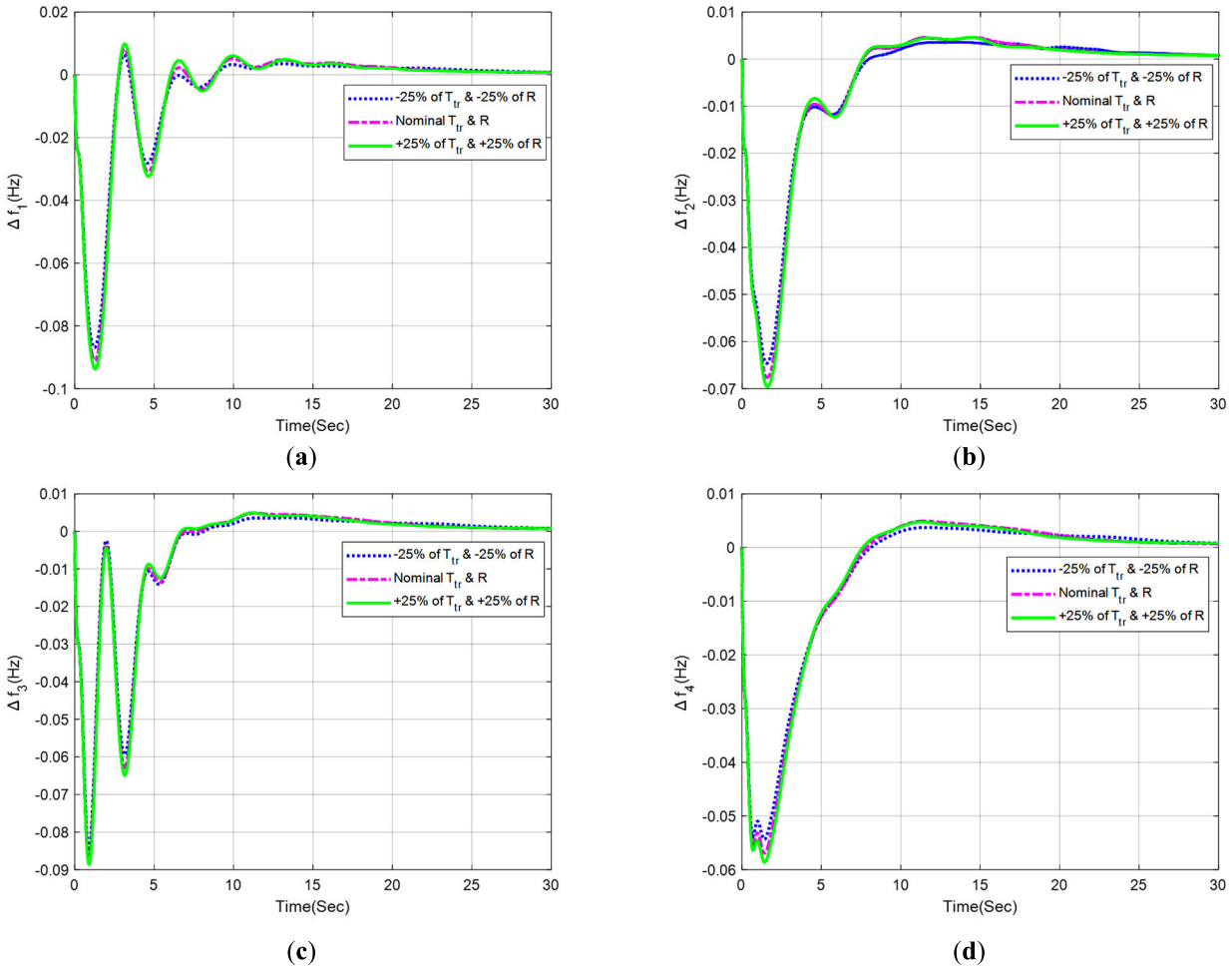

FIGURE 9. LFC responses with ±25% variations in system parameters (a)Δ f1(b)Δ f2(c)Δ f3(d)Δf4.

iteration, the updated position values of the previous iteration are taken to perform further updates. The process goes on till the algorithm reaches the OOBO stopping rule and it returns the quasi-optimal values after full implementation of the algorithm, The pseudo-code for the algorithm is shown below

5) COMPUTATIONAL COMPLEXITY OF OOBO

After the OOBO returns the quasi-optimal values of the optimization problem, the next step is to evaluate the computational complexity of the algorithm. The time complexity of OOBO is affected by the initialization, updating, and cost function evaluation process.

1. Since each the member of population is involved in OOBO so initialization of the population of N size and m decision variables, the initialization time is O(Nm)
2. During the update process, the objective function of N population members is evaluated at each iteration, so the time of update activity is O(NT) where T is the time of each iteration.
3. The update time for the population members is O(NTm)

Algorithm 1 Pseudocode of OOBO

Start OOBO.
1. Input optimization problem information.
2. Set N and T.
3. Create an initial population matrix.
4. Evaluate the objective function.
5. for $t \leftarrow 1$ to T do
6. Update $\vec{K}$ based on Equation (9).
7. for $i \leftarrow 1$ to N do
8. Calculate X_i^{new} based on Equations (10) and (11).
9. Compute f_i^{new} based on X_i^{new}.
10. Update X_i using Equation (12).
11. end for
12. Save the best solution found so far.
13. end for
14. Output the best quasi-optimal solution.

End OOBO.

The time complexity of the OOBO algorithm comes out to be O(N(T(1+m)+m)) which can be written as O(NTm). The space complexity of the OOBO algorithm is O(Nm).

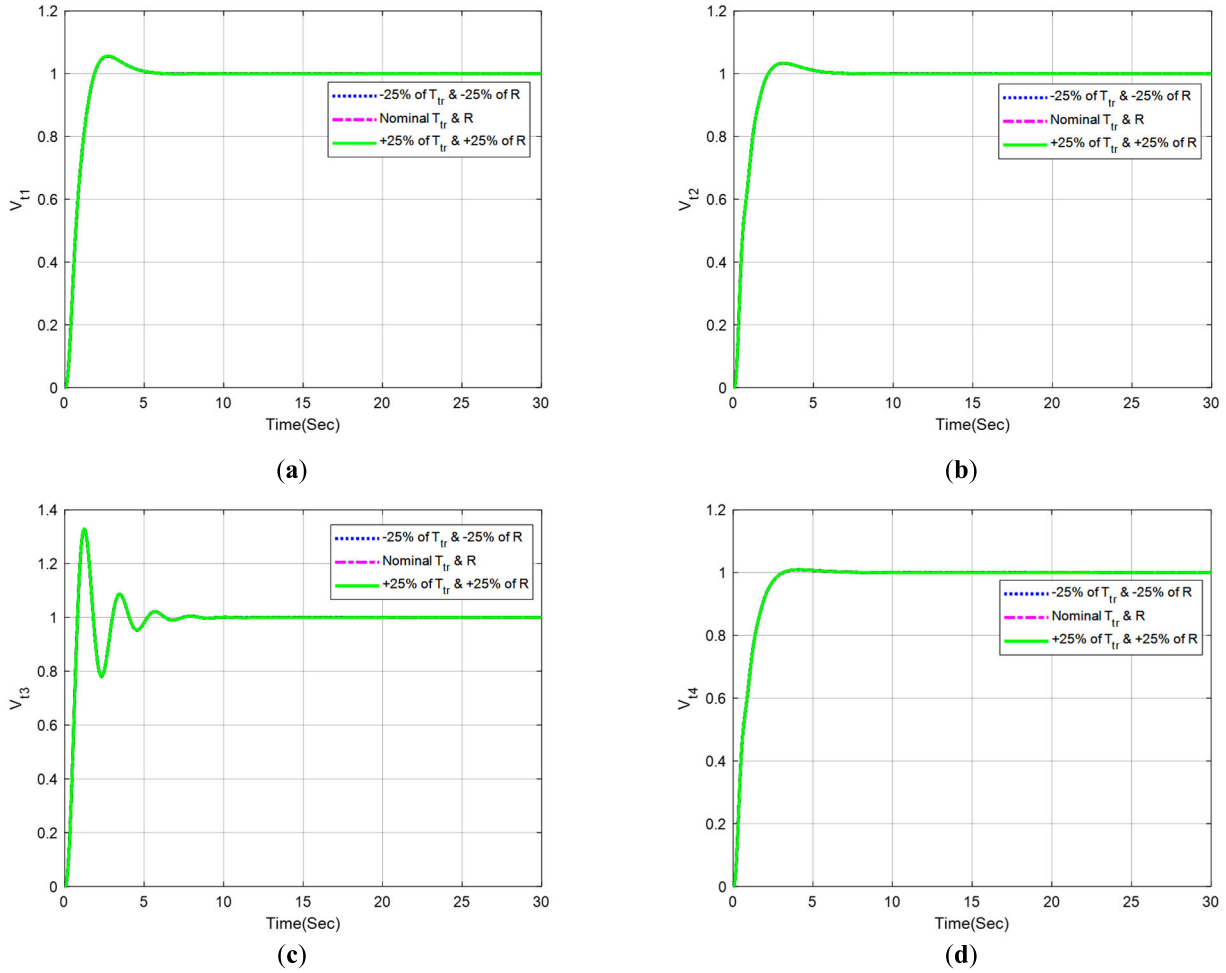

FIGURE 10. AVR responses with ±25% variations in system parameters:(a) Vt1; (b) Vt2; (c) Vt3; (d) Vt4.

IV. SIMULATIONS AND DISCUSSION OF RESULT

Extensive simulations have been conducted in MATLAB/Simulink to validate the suggested control strategy. The rated power of the system is considered 2000MW and the models of generation units have been taken from [38]. First, a four-area, multi-source IPS with 5% SLP (0.05 p.u.) and nonlinearities such as GRC and GDB in thermal reheat and hydropower plants have been considered in each area. Moreover, BD has also been incorporated in thermal reheat power plants for more realistic study. OOBO-based control strategies such as OOBO-PID, OOBO-I-P, OOBO-I-PD, and OOBO-PI-PD have been employed for the optimal control of four-area IPS under such constraints. Then, by changing the system parameters to ±25% in each of the four areas, a detailed sensitivity analysis was also carried out. The OOBO population consists of fifteen solutions whereas five iterations were considered in each simulation to obtain the optimal solution. The lower and upper bounds of solution members are 0.01 and 2 respectively. The step input per unit was taken as reference terminal voltage.

A. FOUR-AREA IPS WITH COMBINED AVR-LFC IN THE PRESENCE OF NONLINEARITIES

The four-area IPS model with nonlinearities under investigation is shown in Figure 1. The system parameters of the four-area IPS are given in Appendix A [38]. The optimal parameters of OOBO-PID, OOBO-I-P, OOBO-I-PD, and OOBO-PI-PD control strategies are given in Table 3. This section presents a detailed comparison of the proposed OOBO-PID, OOBO-I-P, OOBO-I-PD, and OOBO-PI-PD control strategies. Figure 6 displays the frequency deviation response curves, while Table 4 presents the numerical results of LFC performance specifications for each of the four areas utilizing the OOBO-PID, OOBO-I-P, OOBO-I-PD, and OOBO-PI-PD control strategies.

It can be observed that the proposed OOBO-PID control strategy delivered highly satisfactory LFC responses in terms of settling time in each area. OOBO-PID provided settling times of 8.24s, 8.23s, 8.24s, and 8.21s in area-1, area-2, area-3, and area-4 LFC, respectively, which are better than OOBO-I-P, OOBO-I-PD, and OOBO-PI-PD control

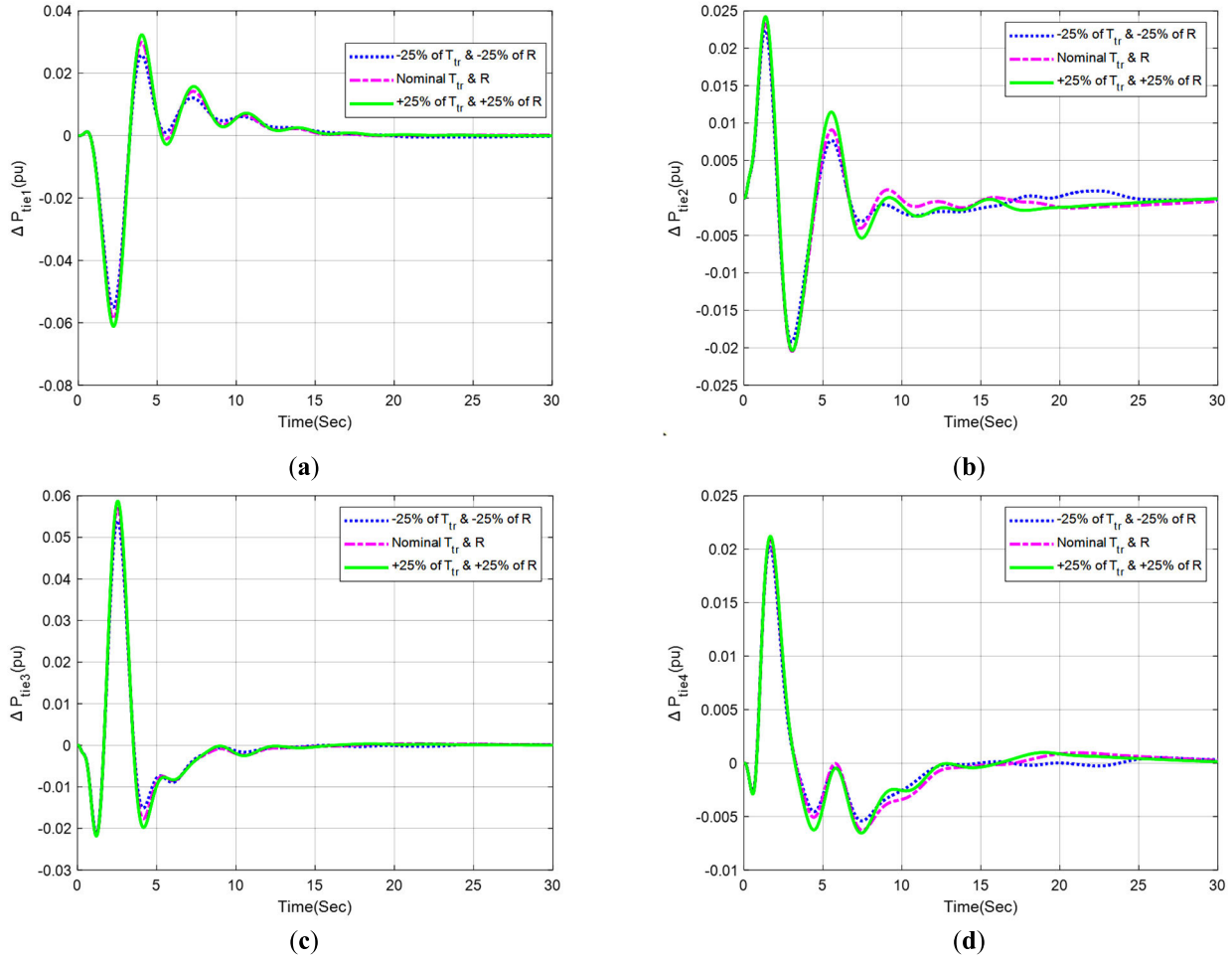

FIGURE 11. Tie-line power deviation responses with ±25% variations in system parameters: (a)Δ Ptie1; (b)Δ Ptie2; (c)Δ Ptie3; (d)Δ Ptie4.

strategies at the cost of percent (%) overshoot and undershoot in each area. OOBO-PI-PD provided a relatively better % overshoot response (0.008, 0.005, 0.0048, and 0.0049) in area-1, area-2, area-3, and area-4 LFC, respectively than OOBO-PID, OOBO-I-P, and OOBO-I-PD control strategies. OOBO-PI-PD yielded a better undershoot response (−0.068) compared to other control strategies in area-2 LFC. OOBO-I-PD provided relatively better undershoot response (−0.053, −0.045, and −0.0052) in area-1, area-3, and area-4 LFC, respectively as compared to OOBO-PID, OOBO-I-P, and OOBO-PI-PD control strategies. The steady-state error is zero with all control strategies in each area.

Figure 7 displays the terminal voltage response curves, while Table 5 presents the numerical results of AVR performance specifications obtained in areas 1, 2, 3, and 4 utilizing the OOBO-PID, OOBO-I-P, OOBO-I-PD, and OOBO-PI-PD control strategies, respectively. For area-1 and area-3 AVR, OOBO-PID provided a settling time of 3.35s and 2.07s which are quicker than OOBO-I-P, OOBO-I-PD, and OOBO-PI-PD control strategies. For area-2 AVR, OOBO-I-PD provided a settling time of 4.18s which is quicker than OOBO-PID, OOBO-I-P, and OOBO-PI-PD control strategies. For area-4 AVR, OOBO-PI-PD provided a settling time of 2.62s which is quicker than OOBO-PID, OOBO-I-P, and OOBO-I-PD control strategies. OOBO-PI-PD provided 5.61% and 3.35% overshoot in area-1 and area-2 AVR which is better than OOBO-PID, OOBO-I-P, and OOBO-I-PD control strategies. OOBO-I-P yielded a zero %overshoot in area-3 whereas OOBO-I-PD provided a 0.44% overshoot in area-4 AVR which is better than OOBO-PID, OOBO-I-PD and OOBO-PI-PD control strategies. The steady-state error is zero with all control strategies.

The tie-line power deviation responses are shown in Figure 8, while the numerical results of tie-line power's performance specifications for areas 1, 2, 3, and 4 are presented in Table 6. OOBO-PI-PD provided settling times of 14.74s and 11.8s in area-1 and area-3, which are better than OOBO-PID, OOBO-I-P, and OOBO-I-PD control strategies. OOBO-PID provided settling times of 11.93s and 9s in area-2 and area-2, which are better than OOBO-I-P, OOBO-I-PD, and OOBO-PI-PD control strategies. OOBO-PID provided relatively better % overshoot response (0.004, 0.015 and 0.019) in area-1, area-2, and area-3 LFC, respectively than OOBO-I-P, OOBO-I-PD, and OOBO-PI-PD control strategies. OOBO-PI-PD yielded a better % overshoot response (0.021) compared to other control strategies in area 4.

OOBO-PID yielded better undershoot responses (−0.009 and −0.016) in area 1 and area 2, which are relatively better than OOBO-I-P, OOBO-I-PD, and OOBO-PI-PD control strategies. OOBO-PI-PD yielded better undershoot responses (−0.022 and −0.0063) in area 3 and area 4, which are relatively better than OOBO-PID, OOBO-I-P, and OOBO-I-PD control strategies. Moreover, OOBO-I-PD provided oscillatory responses in each area which resulted in late settlement of the system response.

B. SENSITIVITY ANALYSIS

In this section, the suggested OOBO-PI-PD control strategy's robustness was evaluated in a four-area IPS with a combined LFC-AVR system. The speed regulation (R) and turbine time constant (T_{tr}) were simultaneously changed to Â ± 25% of their nominal values. In this investigation, the OOBO-PI-PD controller's optimal parameters are taken from Section 5.1. Figures 9-11 illustrate the load frequency, terminal voltage, and tie-lie power responses of the OOBO-PI-PD control strategy with variations in T_{tr} and R, while Tables 7-9 show the numerical results of LFC's dynamic performance specifications, respectively. Despite the ±25% variance in system parameters, it is clear from the results that terminal voltage, load frequency, and tie-line power deviation responses are nearly identical to one another. The fact that values of all performance specifications including settling time, %overshoot, undershoot, and steady-state error have barely changed with variation in system parameters is proof that the suggested technique can function well under dynamic circumstances. The results obtained categorically demonstrate that the recommended OOBO-PI-PD controller is quite robust and does not require retuning for Â ± 25% variations in T_{tr} and R.

V. CONCLUSION

This study thoroughly examined the transient and steady-state performance of a four-area interconnected power system (IPS) with various nonlinearities such as governor dead band (GDB), generation rate constraint (GRC), and boiler dynamics (BD). The research demonstrated that the OOBO-PI-PD controller, optimized with the OOBO algorithm, outperformed other controllers (OOBO-PID, OOBO-I-P, and OOBO-I-PD) in stabilizing terminal voltage, frequency deviations, and tie-line power deviations. Key improvements were observed in overshoot and undershoot responses, with OOBO-PI-PD showing superior performance across different metrics. An extensive sensitivity analysis with ± 25% variations in system parameters demonstrated the robustness of OOBO-PI-PD. The results unequivocally show that the recommended OOBO-PI-PD control strategy is superior for the simultaneous regulation of terminal voltage and load frequency in multi-area IPS. In the future, the suggested methodology can be investigated for controlling the terminal voltage and load frequency simultaneously in a four-area IPS with random loading conditions and a deregulated environment. Moreover, advanced state-of-the-art artificial intelligence and machine learning-based control methods can also be employed to control sophisticated power systems under load-varying conditions with ease.

ACKNOWLEDGMENT

This work was supported by the Deanship of Scientific Research at Northern Border University, Arar, Saudi Arabia, under Project ''NBU-FFR-2024-2448-01''.

REFERENCES

[1] T. Ali, S. A. Malik, I. A. Hameed, A. Daraz, H. Mujlid, and A. T. Azar, ''Load frequency control and automatic voltage regulation in a multi-area interconnected power system using nature-inspired computation-based control methodology,'' *Sustainability*, vol. 14, no. 19, p. 12162, Sep. 2022, doi: 10.3390/su141912162.

[2] T. Ali, S. A. Malik, A. Daraz, S. Aslam, and T. Alkhalifah, ''Dandelion optimizer-based combined automatic voltage regulation and load frequency control in a multi-area, multi-source interconnected power system with nonlinearities,'' *Energies*, vol. 15, no. 22, p. 8499, Nov. 2022, doi: 10.3390/en15228499.

[3] K. Bano, G. Abbas, M. Hatatah, E. Touti, A. Emara, and P. Mercorelli, ''Phase shift APOD and POD control technique in multi-level inverters to mitigate total harmonic distortion,'' *Mathematics*, vol. 12, no. 5, p. 656, Feb. 2024, doi: 10.3390/math12050656.

[4] M. Gupta, S. Srivastava, and J. R. P. Gupta, ''A novel controller for model with combined LFC and AVR loops of single area power system,'' *J. Inst. Eng., India B*, vol. 97, no. 1, pp. 21–29, Mar. 2016, doi: 10.1007/s40031-014-0159-z.

[5] D. Sharma, V. Kushwaha, K. Pandey, and N. Rani, ''Intelligent AVR control of a single thermal area combined with LFC loop,'' in *Intelligent Communication, Control and Devices* (Advances in Intelligent Systems and Computing), 2018, pp. 779–789, doi: 10.1007/978-981-10-5903-2_80.

[6] B. Ali, G. Abbas, A. Memon, S. Mirsaeidi, M. A. Koondhar, S. Chandio, and I. A. Channa, ''A comparative study to analyze wind potential of different wind corridors,'' *Energy Rep.*, vol. 9, pp. 1157–1170, Dec. 2023.

[7] D. K. Lal and A. K. Barisal, ''Combined load frequency and terminal voltage control of power systems using moth flame optimization algorithm,'' *J. Electr. Syst. Inf. Technol.*, vol. 6, no. 1, pp. 1–24, Dec. 2019, doi: 10.1186/s43067-019-0010-3.

[8] A. Ali, A. Shah, M. U. Keerio, N. H. Mugheri, G. Abbas, E. Touti, M. Hatatah, A. Yousef, and M. Bouzguenda, ''Multi-objective security constrained unit commitment via hybrid evolutionary algorithms,'' *IEEE Access*, vol. 12, pp. 6698–6718, 2024, doi: 10.1109/ACCESS.2024.3351710.

[9] J. Morsali and Z. Esmaeili, ''Proposing a new hybrid model for LFC and AVR loops to improve effectively frequency stability using coordinative CPSS,'' in *Proc. 28th Iranian Conf. Electr. Eng. (ICEE)*, Tabriz, Iran, Aug. 2020, pp. 1–7, doi: 10.1109/ICEE50131.2020.9260695.

[10] C. N. S. Kalyan and G. S. Rao, ''Frequency and voltage stabilisation in combined load frequency control and automatic voltage regulation of multiarea system with hybrid generation utilities by AC/DC links,'' *Int. J. Sustain. Energy*, vol. 39, no. 10, pp. 1009–1029, Nov. 2020, doi: 10.1080/14786451.2020.1797740.

[11] C. N. S. Kalyan and G. S. Rao, ''Combined frequency and voltage stabilisation of multi-area multisource system by DE-AEFA optimised PID controller with coordinated performance of IPFC and RFBs,'' *Int. J. Ambient Energy*, vol. 43, no. 1, pp. 3815–3831, Dec. 2022, doi: 10.1080/01430750.2020.1860130.

[12] A. Ali, G. Abbas, M. U. Keerio, M. A. Koondhar, K. Chandni, and S. Mirsaeidi, ''Solution of constrained mixed-integer multi-objective optimal power flow problem considering the hybrid multi-objective evolutionary algorithm,'' *IET Gener., Transmiss. Distrib.*, vol. 17, no. 1, pp. 66–90, Jan. 2023, doi: 10.1049/gtd2.12664.

[13] N. Nahas, M. Abouheaf, M. N. Darghouth, and A. Sharaf, ''A multi-objective AVR-LFC optimization scheme for multi-area power systems,'' *Electric Power Syst. Res.*, vol. 200, Nov. 2021, Art. no. 107467, doi: 10.1016/j.epsr.2021.107467.

[14] C. N. S. Kalyan, ''UPFC and SMES based coordinated control strategy for simultaneous frequency and voltage stability of an interconnected power system,'' in *Proc. 1st Int. Conf. Power Electron. Energy (ICPEE)*, Bhubaneswar, India, Jan. 2021, pp. 1–6, doi: 10.1109/ICPEE50452.2021.9358576.

[15] P. Anusha, S. Patra, A. Roy, and D. Saha, "Combined frequency and voltage control of a deregulated hydro-thermal power system employing FA based industrial controller," in *Proc. Int. Conf. Comput. Perform. Eval. (ComPE)*, Shillong, India, Dec. 2021, pp. 848–853, doi: 10.1109/ComPE53109.2021.9752331.
[16] S. Oladipo, Y. Sun, and Z. Wang, "An effective hFPAPFA for a PIDA-based hybrid loop of load frequency and terminal voltage regulation system," in *Proc. IEEE PES/IAS PowerAfrica*, Nairobi, Kenya, Aug. 2021, pp. 1–5, doi: 10.1109/powerafrica52236.2021.9543348.
[17] S. K. Ramoji and L. C. Saikia, "Optimal coordinated frequency and voltage control of CCGT-thermal plants with TIDF controller," *IETE J. Res.*, vol. 69, no. 7, pp. 4836–4853, Sep. 2023, doi: 10.1080/03772063.2021.1959420.
[18] A. Ali, Z. Liu, A. Ali, G. Abbas, E. Touti, and W. Nureldeen, "Dynamic multi-objective optimization of grid-connected distributed resources along with battery energy storage management via improved bidirectional coevolutionary algorithm," *IEEE Access*, vol. 12, pp. 58972–58992, 2024, doi: 10.1109/ACCESS.2024.3392911.
[19] S. K. Ramoji, L. C. Saikia, B. Dekaraja, M. K. Behera, and S. K. Bhagat, "Performance comparison of various tilt controllers in coalesced voltage and frequency regulation of multi-area multi-unit power system," in *Proc. IEEE Delhi Sect. Conf. (DELCON)*, New Delhi, India, Feb. 2022, pp. 1–7, doi: 10.1109/DELCON54057.2022.9752811.
[20] S. Habib, G. Abbas, T. A. Jumani, A. A. Bhutto, S. Mirsaeidi, and E. M. Ahmed, "Improved whale optimization algorithm for transient response, robustness, and stability enhancement of an automatic voltage regulator system," *Energies*, vol. 15, no. 14, p. 5037, Jul. 2022, doi: 10.3390/en15145037.
[21] B. Dekaraja, L. C. Saikia, and S. K. Ramoji, "Combined ALFC-AVR control of diverse energy source based interconnected power system using cascade controller," in *Proc. Int. Conf. Intell. Controller Comput. for Smart Power (ICICCSP)*, Hyderabad, India, Jul. 2022, pp. 1–6, doi: 10.1109/ICICCSP53532.2022.9862433.
[22] A. Hafeez, A. Ali, M. U. Keerio, N. H. Mugheri, G. Abbas, A. Khan, S. Mirsaeidi, A. Yousef, E. Touti, and M. Bouzguenda, "Optimal site and size of FACTS devices with the integration of uncertain wind generation on a solution of stochastic multi-objective optimal power flow problem," *Frontiers Energy Res.*, vol. 11, Nov. 2023, Art. no. 1293870.
[23] H. H. Fayek and E. Rusu, "Novel combined load frequency control and automatic voltage regulation of a 100% sustainable energy interconnected microgrids," *Sustainability*, vol. 14, no. 15, p. 9428, Aug. 2022, doi: 10.3390/su14159428.
[24] C. N. S. Kalyan, B. S. Goud, C. R. Reddy, M. Bajaj, N. K. Sharma, H. H. Alhelou, P. Siano, and S. Kamel, "Comparative performance assessment of different energy storage devices in combined LFC and AVR analysis of multi-area power system," *Energies*, vol. 15, no. 2, p. 629, Jan. 2022, doi: 10.3390/en15020629.
[25] A. Ali, A. Hassan, M. U. Keerio, N. H. Mugheri, G. Abbas, M. Hatatah, E. Touti, and A. Yousef, "A novel solution to optimal power flow problems using composite differential evolution integrating effective constrained handling techniques," *Sci. Rep.*, vol. 14, no. 1, p. 6187, Mar. 2024.
[26] Y. Arya, "ICA assisted FTIλDN controller for AGC performance enrichment of interconnected reheat thermal power systems," *J. Ambient Intell. Humanized Comput.*, vol. 14, no. 3, pp. 1919–1935, Mar. 2023, doi: 10.1007/s12652-021-03403-6.
[27] A. Daraz, S. A. Malik, A. Waseem, A. T. Azar, I. U. Haq, Z. Ullah, and S. Aslam, "Automatic generation control of multi-source interconnected power system using FOI-TD controller," *Energies*, vol. 14, no. 18, p. 5867, Sep. 2021, doi: 10.3390/en14185867.
[28] G. Abbas, W. Zhi, and A. Ali, "A two-stage reactive power optimization method for distribution networks based on a hybrid model and data-driven approach," *IET Renew. Power Gener.*, Aug. 2024, doi: 10.1049/rpg2.13096.
[29] A. Daraz, S. A. Malik, H. Mokhlis, I. U. Haq, F. Zafar, and N. N. Mansor, "Improved-fitness dependent optimizer based FOI-PD controller for automatic generation control of multi-source interconnected power system in deregulated environment," *IEEE Access*, vol. 8, pp. 197757–197775, 2020, doi: 10.1109/ACCESS.2020.3033983.
[30] A. Daraz, S. A. Malik, A. T. Azar, S. Aslam, T. Alkhalifah, and F. Alturise, "Optimized fractional order integral-tilt derivative controller for frequency regulation of interconnected diverse renewable energy resources," *IEEE Access*, vol. 10, pp. 43514–43527, 2022, doi: 10.1109/ACCESS.2022.3167811.
[31] G. Abbas, Z. Wu, and A. Ali, "Multi-objective multi-period optimal site and size of distributed generation along with network reconfiguration," *IET Renew. Power Gener.*, Feb. 2024, doi: 10.1049/rpg2.12949.
[32] H. H. Coban, A. Rehman, and M. Mousa, "Load frequency control of microgrid system by battery and pumped-hydro energy storage," *Water*, vol. 14, no. 11, p. 1818, Jun. 2022, doi: 10.3390/w14111818.
[33] A. Tabak, "Maiden application of fractional order PID plus second order derivative controller in automatic voltage regulator," *Int. Trans. Electr. Energy Syst.*, vol. 31, no. 12, Dec. 2021, Art. no. e13211, doi: 10.1002/2050-7038.13211.
[34] A. Tabak, "A novel fractional order PID plus derivative ($PI^{\lambda}D^{\mu}D^{\mu 2}$) controller for AVR system using equilibrium optimizer," *COMPEL Int. J. Comput. Math. Electr. Electron. Eng.*, vol. 40, no. 3, pp. 722–743, 2021, doi: 10.1108/compel-02-2021-0044.
[35] A. K. V. Krishna and T. Tyagi, "Improved whale optimization algorithm for numerical optimization," in *Advances in Computational Intelligence and Communication Technology* (Advances in Intelligent Systems and Computing), vol. 1086, 2021, pp. 59–71, doi: 10.1007/978-981-15-1275-9_6.
[36] S. M. A. Altbawi, A. S. B. Mokhtar, T. A. Jumani, I. Khan, N. N. Hamadneh, and A. Khan, "Optimal design of fractional order PID controller based automatic voltage regulator system using gradient-based optimization algorithm," *J. King Saud Univ., Eng. Sci.*, vol. 36, no. 1, pp. 32–44, Jan. 2024, doi: 10.1016/j.jksues.2021.07.009.
[37] G. Abbas, Z. Wu, and A. Ali, "Optimal scheduling and management of grid-connected distributed resources using improved decomposition-based many-objective evolutionary algorithm," *IET Gener., Transmiss. Distrib.*, vol. 18, no. 16, pp. 2625–2649, Aug. 2024, doi: 10.1049/gtd2.13221.
[38] T. Ali, S. A. Malik, A. Daraz, M. Adeel, S. Aslam, and H. Herodotou, "Load frequency control and automatic voltage regulation in four-area interconnected power systems using a gradient-based optimizer," *Energies*, vol. 16, no. 5, p. 2086, Feb. 2023.
[39] A. Ali, G. Abbas, M. U. Keerio, E. Touti, Z. Ahmed, O. Alsalman, and Y.-S. Kim, "A bi-level techno-economic optimal reactive power dispatch considering wind and solar power integration," *IEEE Access*, vol. 11, pp. 62799–62819, 2023.
[40] R. Sepehrzad, A. Hedayatnia, M. Amohadi, J. Ghafourian, A. Al-Durra, and A. Anvari-Moghaddam, "Two-stage experimental intelligent dynamic energy management of microgrid in smart cities based on demand response programs and energy storage system participation," *Int. J. Electr. Power Energy Syst.*, vol. 155, Jan. 2024, Art. no. 109613.
[41] R. Sepehrzad, J. Ghafourian, A. Hedayatnia, A. Al-Durrad, and M. H. Khooban, "Experimental and developed DC microgrid energy management integrated with battery energy storage based on multiple dynamic matrix model predictive control," *J. Energy Storage*, vol. 74, Dec. 2023, Art. no. 109282.
[42] A. Ali, S. Aslam, S. Mirsaeidi, N. H. Mugheri, R. H. Memon, G. Abbas, and H. Alnuman, "Multi-objective multiperiod stable environmental economic power dispatch considering probabilistic wind and solar PV generation," *IET Renew. Power Gener.*, Aug. 2024, doi: 10.1049/rpg2.13077.
[43] M. E. Hassanzadeh, M. Nayeripour, S. Hasanvand, and R. Sepehrzad, "Hierarchical optimal allocation of BESS using APT-FPSO based on stochastic programming model considering voltage sensitivity and eigenvalues analyses," *Int. J. Electr. Power Energy Syst.*, vol. 153, Nov. 2023, Art. no. 109291.
[44] A. Ali, G. Abbas, M. U. Keerio, S. Mirsaeidi, S. Alshahr, and A. Alshahir, "Pareto front-based multiobjective optimization of distributed generation considering the effect of voltage-dependent nonlinear load models," *IEEE Access*, vol. 11, pp. 12195–12217, 2023, doi: 10.1109/ACCESS.2023.3242546.
[45] P. K. Pathak and A. K. Yadav, "Fuzzy assisted optimal tilt control approach for LFC of renewable dominated micro-grid: A step towards grid decarbonization," *Sustain. Energy Technol. Assessments*, vol. 60, Dec. 2023, Art. no. 103551.
[46] P. K. Pathak, A. K. Yadav, S. Padmanaban, and I. Kamwa, "Fractional cascade LFC for distributed energy sources via advanced optimization technique under high renewable shares," *IEEE Access*, vol. 10, pp. 92828–92842, 2022.
[47] J. Khalid, M. A. M. Ramli, M. S. Khan, and T. Hidayat, "Efficient load frequency control of renewable integrated power system: A twin delayed DDPG-based deep reinforcement learning approach," *IEEE Access*, vol. 10, pp. 51561–51574, 2022.

[48] M. Dehghani, E. Trojovská, P. Trojovský, and O. P. Malik, "OOBO: A new metaheuristic algorithm for solving optimization problems," *Biomimetics*, vol. 8, no. 6, p. 468, 2023.

TAYYAB ALI is currently with the Department of Electrical and Computer Engineering, International Islamic University Islamabad, Pakistan. His research interests include renewable energy, control of electrical systems smart grids, electric vehicles, and power electronics.

MUHAMMAD ASAD is currently with the Department of Electrical and Computer Engineering, International Islamic University Islamabad, Pakistan. His research interests include renewable energy, control of electrical systems smart grids, electric vehicles, and power electronics.

EZZEDDINE TOUTI received the B.S. degree in electrical engineering from the Higher National College of Engineers of Tunis, Tunisia, in 1997, the master's degree in electrical engineering from the National College of Engineers of Tunis, Tunisia, in 2005, and the joint Ph.D. degree in induction generators wind turbine, power quality and electric drives from the National College of Engineers of Monastir, Tunisia, and Artois University, France, in 2013. In 2005, he joined the Laboratory of Industrial Systems Engineering and Renewable Energies (LISIER), University of Tunis, Tunisia, as a Researcher Faculty Member. He is currently an Associate Professor with the College of Engineering, Northern Border University. His research interests include renewable energy, control of electrical systems smart grids, electric vehicles, and power electronics.

BESMA BECHIR GRABA is currently an Assistant Professor with the Department of Physics, College of Science, Northern Border University, Arar, Saudi Arabia. Her research interests include renewable energy and electrical systems smart grids.

MOULOUD AOUDIA is currently an Assistant Professor and an Associate Professor with the Department of Industrial Engineering, College of Engineering, Northern Border University, Arar, Saudi Arabia.

GHULAM ABBAS received the B.Eng. degree in electrical engineering from QUEST, Nawabshah, Pakistan, in 2017, and the M.Eng. degree in electrical engineering from Southeast University, Nanjing, China, in 2019, where he is currently pursuing the Ph.D. degree in electrical engineering. His research interests include distributed generation integration, planning, and optimization.

HAMMAD ALNUMAN received the B.S. degree in electrical engineering from Jouf University, Al Jouf, Saudi Arabia, in 2012, the M.S. degree in electrical and computer engineering from Southern Illinois University, Carbondale, IL, USA, in 2014, and the Ph.D. degree in electronic and electrical engineering from The University of Sheffield, Sheffield, U.K., in 2021. He is currently an Assistant Professor at Jouf University. His research interests include energy efficiency in electric railways, railways simulation, railways operation and control, hybrid energy storage systems for integrated energy applications, renewable energy applications, and micro-grids.

WALEED NURELDEEN is currently an Assistant Professor with the College of Engineering, University of Business and Technology, Jeddah, Saudi Arabia.